

AN OVERVIEW OF THE IMMERSSED INTERFACE METHOD AND ITS APPLICATIONS*

Zhilin Li

Abstract. Interface problems have many applications. Mathematically, interface problems usually lead to differential equations whose input data and solutions are non-smooth or discontinuous across some interfaces. The immersed interface method (IIM) has been developed in recent years particularly designed for interface problems. The IIM is a sharp interface method based on Cartesian grids. The IIM makes use of the jump conditions across the interface so that the finite difference/element discretization can be accurate. In this survey paper, we will introduce the immersed interface method for various problems, discuss its recent advances and related software packages, and some of its applications. We also review some other related methods and references in this survey paper.

1. INTRODUCTION

Interface problems are those problems in which the input data (such as the coefficients of differential equations, source terms etc.) may be discontinuous or even singular across one or several interfaces in the solution domain. The solution to an interface problem, therefore, typically is non-smooth or even discontinuous across the interfaces.

Interface problems have attracted a lot of attention from both theoretical and numerical analysts over the years. Mathematically, interface problems

Received July 31, 2002.

Communicated by S. B. Hsu.

2000 *Mathematics Subject Classification*: 65N06, 65N50.

Key words and phrases: Interface problems, Immersed interface method, Immersed boundary method, Delta function, Discontinuous coefficients, Level set method, Maximum principle preserving scheme, Non-linear interface problems, Finite difference, Finite element method.

*The author was supported in part by ARO grants, 39676-MA and 43751-MA, and NSF grants, DMS-00-0073403 and DMS-02-01094, USA.

usually lead to differential equations whose input data and solutions are non-smooth or discontinuous across some interfaces. Many numerical methods designed for smooth solutions do not work, or work poorly, for interface problems.

Interface problems occur in many physical applications, particularly for free boundary/moving interface problems, for examples, the modeling of the Stefan problem of solidification process and crystal growth, composite materials, multi-phase flows, cell and bubble deformation, and many others. We present a model problem below to show the importance and characteristics of the interface problems of our interest. More examples will be discussed later in this paper.

1-1. A model problem and analysis

The heat equation

$$(1.1) \quad u_t = (\beta u_x)_x + f(x, t)$$

describes many physical phenomena. For instance, u may represent the temperature distribution in a material with heat conductivity β . If there are two different materials that meets at $x = \alpha$, then the coefficient β is discontinuous across the interface $x = \alpha$ between the different materials, see [52] for an example. Physically, the temperature should be continuous, which means $[u] = 0$ across the interface, where

$$(1.2) \quad [u] = \lim_{x \rightarrow \alpha^+} u(x) - \lim_{x \rightarrow \alpha^-} u(x) = u^+ - u^-$$

denotes the jump of $u(x)$ at the interface α . We distinguish the following situations:

- The source term $f(x, t)$ is continuous, but the coefficient β is not. Then the heat flux is continuous, *i.e.*, $[\beta u_x] = 0$, but u_x is not unless it vanishes at the interface α .
- The source term is singular with $f(x, t) = C(t) \delta(x - \alpha)$, in other words there is a point source at α . So the heat flux at α has a jump given by the source strength $C(t)$, *i.e.*, $[\beta u_x] = -C(t)$. In this case, u_x is discontinuous even if β is continuous.
- The steady state case is: $(\beta u_x)_x = -f(x)$. In particular, suppose $f(x) = C \delta(x - \alpha)$ and β is constant on each side of the interface α , then the solution is a piecewise linear function, see Fig. 2.1 for an example. Even for this simplest example, special care has to be taken to deal with the discontinuity in β and the delta function singularity when we want to solve the problem numerically.

The immersed interface method (IIM) has been developed for solving the following problems:

- The differential equation/system has discontinuous but bounded coefficients.
- The differential equation/system has singular source term such as a Dirac delta function.
- The interface can be fixed or moving with time.
- There are one or several interfaces.
- Problems that are defined on irregular domains.

In all of the cases above except for the last one, the solution can be discontinuous, for example, the pressure of the Navier-Stokes equations involving interfaces (see Sec. 9.1), or non-smooth, for example, the temperature in the heat equation involving interfaces.

For an elliptic interface problem of the form

$$(1.3) \quad \nabla \cdot (\beta(\mathbf{x})\nabla u) - \kappa(\mathbf{x})u = f(\mathbf{x}), \quad \mathbf{x} \in \Omega,$$

the solution $u(\mathbf{x})$ generally is not in $H^2(\Omega)$ if $\beta(\mathbf{x})$ and $\kappa(\mathbf{x})$ have discontinuities even if $f(\mathbf{x}) \in L^2(\Omega)$. The existence and uniqueness of the weak solution is discussed in [7, 12]. The conclusion is that the solution is in *piecewise* $H^2(\Omega)$. However, in many practical applications, it is reasonable to assume that the solution is piecewise smooth in the neighborhood of the interface if the interface is smooth.

To solve an interface problem numerically, usually we need to choose a grid first. In general, there are two kinds of grids: (i) a body fitted grid that is usually combined with a finite element (FE) method, see for example, [7, 12]; (ii) a Cartesian grid that is usually associated with a finite difference (FD) discretization.

The immersed interface method is often based on a *Cartesian grid* and is often associated with a finite difference method. However, it has been also combined with finite element methods [43, 45].

1.2. Why Cartesian grids?

One of obvious advantages of using Cartesian grids is that there is almost no cost for the grid generation. Also conventional numerical schemes can be used at most grid points that are away from the interface since there are no irregularities there. Only those grid points near the interface, which are usually much fewer than regular grid points, need special attention.

Another advantage of using Cartesian grids is that we can take advantage of many software packages or methods developed for Cartesian grids, for example, the fast Poisson solvers [77], the Clawpack [35] and the Amrclawpack [4], the level set method [61], the structured multigrid solvers [1, 14], the immersed boundary method [64], and many others.

More importantly, we are interested primarily in time-dependent problems, and the interfaces are typically moving. Although it is possible to develop moving mesh methods that conform to the interfaces in each time step, this is generally much more complicated than simply allowing the interface to move relative to a fixed underlying grid.

1.3. Some commonly used methods for interface problems

In the discussion below, we assume a uniform Cartesian grid x_i , $i = 1, 2, \dots$, with the step size $h = x_i - x_{i-1}$.

1.3-1. The smoothing method for discontinuous coefficients

In one space dimension, let $\beta(x)$ be a function that has a finite jump at $x = \alpha$, i.e., $[\beta] = \lim_{x \rightarrow \alpha^+} \beta(x) - \lim_{x \rightarrow \alpha^-} \beta(x) \neq 0$. Define

$$(1.4) \quad \beta^-(x) = \begin{cases} \beta(x), & \text{if } x < \alpha, \\ 0, & \text{if } x > \alpha, \end{cases} \quad \beta^+(x) = \begin{cases} 0, & \text{if } x < \alpha, \\ \beta(x), & \text{if } x > \alpha. \end{cases}$$

We can smooth $\beta(x)$ using

$$(1.5) \quad \beta_\epsilon(x) = \beta^-(x) + (\beta^+(x) - \beta^-(x)) H_\epsilon(x - \alpha),$$

where H_ϵ is smoothed Heaviside function

$$(1.6) \quad H_\epsilon(x) = \begin{cases} 0, & \text{if } x < -\epsilon, \\ \frac{1}{2} \left(1 + \frac{x}{\epsilon} + \frac{1}{\pi} \sin \frac{\pi x}{\epsilon} \right), & \text{if } |x| \leq \epsilon, \\ 1, & \text{if } x > \epsilon, \end{cases}$$

and $\epsilon > 0$ is a small number depending on the step size of a numerical scheme, see for example [76]. The coefficient in the front of the sine function is chosen so that $H_\epsilon(x)$ is both continuous and smooth at $x = \pm\epsilon$. The smoothing method is not very accurate, see, for example, Fig. 2.1. It will smooth out the solution as well.

For two or three dimensional problems, the smoothing method may not be so easy to implement unless the interface is expressed as the zero level set of a Lipschitz continuous function $\varphi(\mathbf{x})$. For example, let the set $\{\mathbf{x}, \varphi(\mathbf{x}) = 0\}$

be the interface, then the smoothing function of a discontinuous function $\beta(\mathbf{x})$ is simply $\beta_\epsilon(\varphi(\mathbf{x}))$.

1.3.2. The harmonic averaging for discontinuous coefficients

For elliptic interface problems, another method that is more accurate than the smoothing method for discontinuous coefficients is the *harmonic averaging*, see [3], [75] and [78]. Take the one dimensional expression $(\beta u_x)_x$ as an example. The discrete form of $(\beta u_x)_x$ can be written as

$$\frac{1}{h^2} \left[\beta_{i+\frac{1}{2}}(u_{i+1} - u_i) - \beta_{i-\frac{1}{2}}(u_i - u_{i-1}) \right].$$

If β is smooth then we can take $\beta_{i+\frac{1}{2}} = \beta(x_{i+\frac{1}{2}})$, where $x_{i+\frac{1}{2}} = x_i + h/2$, and the discretization is second order accurate. If β is discontinuous in $[x_{i-1}, x_{i+1}]$, then the harmonic average of $\beta(x)$ is

$$(1.7) \quad \beta_{i+\frac{1}{2}} = \left[\frac{1}{h} \int_{x_i}^{x_{i+1}} \beta^{-1}(x) dx \right]^{-1}.$$

This can be justified by homogenization theory for problems where $\beta(x)$ varies rapidly on the scale of the grid cells. The method using the harmonic averaging is second order accurate in the maximum norm for one dimensional elliptic interface problems due to primarily the result of fortuitous cancellation, see [39]. However, we need to calculate the integral (1.7) accurate enough to guarantee second order accuracy, which is not so easy especially in the interval where the discontinuity takes place.

In two space dimensions, the harmonic averaging is also commonly used to deal with discontinuous coefficients [3], [75], now integrating over squares to obtain the harmonic average of $\beta(x, y)$. In this case, however, the method does not appear to give second order accurate results because the cancellations are very unlikely to take place for arbitrary interfaces. It is also not practical to compute the integrals accurately near the interface in two space dimensions when β is discontinuous.

1.3.3. Peskin's immersed boundary (IB) method

This method was originally developed by Peskin [62, 63] to model blood flow in the heart, and has since been applied to many other problems, particularly in biophysics. We refer the readers to the recent review article [64] for the method and its applications. One of very important ideas in the IB method is the use of a discrete delta function to distribute singular source to

nearby grid points. There are several discrete delta functions in the literature. The commonly used ones include the hat function

$$(1.8) \quad \delta_h(x) = \begin{cases} (h - |x|)/h^2, & \text{if } |x| < h, \\ 0, & \text{if } |x| \geq h, \end{cases}$$

and Peskin's original discrete cosine delta function

$$(1.9) \quad \delta_h(x) = \begin{cases} \frac{1}{4h}(1 + \cos(\pi x/2h)), & \text{if } |x| < 2h, \\ 0, & \text{if } |x| \geq 2h. \end{cases}$$

The two discrete delta functions above are both continuous. The first one is not smooth but the solution obtained by using it gives second order accuracy for some one-dimensional problems [5]. The discrete cosine delta function is smooth but the solution obtained by using it is only first order accurate. The discrete delta function approach is robust and simple to implement. In high dimensions, the discrete delta function used is often the product of one dimensional discrete delta functions, for example, $\delta_h(x, y) = \delta_h(x)\delta_h(y)$.

The original motivation of the immersed interface method is to generalize the results in [5] to two and three dimensional problems and try to improve accuracy of Peskin's IB method. However, it seems unlikely that the discrete delta function approach can achieve second order or higher accuracy except in a few special situations, e.g., when the interface is aligned with a grid line.

The rest of the paper is organized as follows. In the next section, we introduce the IIM for one dimensional problems. The IIM for two dimensional problems are introduced in Sec. 3. In Sec. 4, the fast IIM for piecewise constant coefficients is briefly explained followed by the application to elliptic PDEs defined on irregular domains. We mention some implementation details of the IIM in Sec. 5. The IIM for three dimensional problems are also explained there. Recent work on the IIM in the polar coordinates is discussed in Sec. 6. In Sec. 7, the IIM using the finite element methods with modified basis functions is presented. Some applications of the IIM to interesting physical problems can be found in Sec. 8. Other methods that are related to the IIM is reviewed in Sec. 10. We conclude the paper and point some future research directions in Sec. 11.

2. THE IMMERSSED INTERFACE METHOD FOR 1D ELLIPTIC INTERFACE PROBLEMS

Consider a simple but typical 1D elliptic interface problem

$$(2.1) \quad (\beta u_x)_x - \kappa u = f + C\delta(x - \alpha), \quad 0 < x < 1, \quad 0 < \alpha < 1,$$

with specified boundary conditions on u at $x = 0$ and $x = 1$. The function $\beta(x)$ is allowed to be discontinuous at $x = \alpha$ but $\kappa(x)$ and $f(x)$ are smooth functions for simplicity.

2.1. Reformulating the problem using the jump conditions

By integrating (2.1) from $x = \alpha^-$ to $x = \alpha^+$, we can get

$$(2.2) \quad [u] \Big|_{\alpha} = u^+ - u^- = 0, \quad [\beta u_x] \Big|_{\alpha} = \beta^+ u_x^+ - \beta^- u_x^- = C.$$

An alternative way to state the problem (2.1) is to require that $u(x)$ satisfy the equation

$$(2.3) \quad (\beta u_x)_x - \kappa u = f, \quad x \in (0, \alpha) \cup (\alpha, 1),$$

excluding the interface α , together with the two internal boundary conditions (2.2) at $x = \alpha$. When $f(x)$ is continuous, we also have

$$\beta_x^+ u_x^+ + \beta^+ u_{xx}^+ - \kappa^+ u^+ = \beta_x^- u_x^- + \beta^- u_{xx}^- - \kappa^- u^-.$$

Since we assume that $\kappa^+ = \kappa^-$, $\beta_x^- = \beta_x^+ = 0$, and $u^+ = u^-$, we can express the limiting quantities from + side in terms of those from the - side to get,

$$(2.4) \quad u^+ = u^-, \quad u_x^+ = \frac{\beta^-}{\beta^+} u_x^- + \frac{C}{\beta^+}, \quad u_{xx}^+ = \beta^- u_{xx}^- / \beta^+.$$

2.2. The finite difference equations

The algorithm of the IIM for (2.3) and (2.2) is outlined below. The key derivation is given in the next sub-section.

- Generate a Cartesian grid:

$$x_i = ih, \quad i = 1, 2, \dots, n$$

where $h = 1/n$. The point α will typically fall between the grid points, say $x_j \leq \alpha < x_{j+1}$. The grid points x_j and x_{j+1} are called *irregular grid points*. The other grid points are called regular grid points.

- Determine the finite difference scheme at regular grid points. At a grid points x_i , $i \neq j, j+1$, the standard finite difference approximation

$$(2.5) \quad \frac{1}{h^2} \left(\beta_{i+\frac{1}{2}} (u_{i+1} - u_i) - \beta_{i-\frac{1}{2}} (u_i - u_{i-1}) \right) + \kappa_i u_i = f_i,$$

is used, where $\beta_{i+\frac{1}{2}} = \beta(x_{i+\frac{1}{2}})$, $\kappa_i = \kappa(x_i)$, $f_i = f(x_i)$.

- Determine the finite difference scheme at irregular regular grid points x_j and x_{j+1} . The finite difference equations are determined from the method of undetermined coefficients:

$$(2.6) \quad \begin{aligned} \gamma_{j,1}u_{j-1} + \gamma_{j,2}u_j + \gamma_{j,3}u_{j+1} - \kappa_j u_j &= f_j + C_j, \\ \gamma_{j+1,1}u_j + \gamma_{j+1,2}u_{j+1} + \gamma_{j+1,3}u_{j+2} - \kappa_{j+1}u_{j+1} &= f_{j+1} + C_{j+1}. \end{aligned}$$

For the simple model problem in which $\kappa \equiv 0$, $[f] = 0$, and β is piecewise coefficient, the coefficients of the finite difference have the following closed form:

$$(2.7) \quad \begin{aligned} \gamma_{j,1} &= (\beta^- - [\beta](x_j - \alpha)/h)/D_j, & \gamma_{j+1,1} &= \beta^-/D_{j+1}, \\ \gamma_{j,2} &= (-2\beta^- + [\beta](x_{j-1} - \alpha)/h)/D_j, & \gamma_{j+1,2} &= (-2\beta^+ + [\beta](x_{j+2} - \alpha)/h)/D_{j+1}, \\ \gamma_{j,3} &= \beta^+/D_j, & \gamma_{j+1,3} &= (\beta^+ - [\beta](x_{j+1} - \alpha)/h)/D_{j+1}, \end{aligned}$$

where

$$D_j = h^2 + [\beta](x_{j-1} - \alpha)(x_j - \alpha)/2\beta^-,$$

$$D_{j+1} = h^2 - [\beta](x_{j+2} - \alpha)(x_{j+1} - \alpha)/2\beta^+.$$

It has been shown in [21, 39] that $D_j \neq 0$ and $D_{j+1} \neq 0$ if $\beta^-\beta^+ > 0$. The correction terms are:

$$(2.8) \quad C_j = \gamma_j, 3(x_{j+1} - \alpha) \frac{C}{\beta^+}, \quad C_{j+1} = \gamma_{j+1}, 1(\alpha - x_{j+1}) \frac{C}{\beta^-}.$$

- Solve the tridiagonal system of equations to get an approximate solution of $u(x)$.

Remark 2.1. Note that when $[\beta] = 0$, we recover the standard central finite difference using the three-point stencil, and the correction terms are the same as those obtained from the discrete delta function (1.8).

2.3. A brief derivation of the finite difference scheme at an irregular grid point

We illustrate the idea of the IIM in determining the finite difference coefficients $\gamma_{j,1}$, $\gamma_{j,2}$ and $\gamma_{j,3}$ in (2.6). We want to determine the coefficients so that the local truncation error is as small as possible in the magnitude. The main idea is to expand the solution $u(x_{j-1})$, $u(x_j)$, and $u(x_{j+1})$ at the interface α , then use the interface relation (2.2) to express them in terms of the quantities from one particular side.

Using the Taylor expansion for $u(x_{j+1})$ at α , we have

$$u(x_{j+1}) = u^+(\alpha) + (x_{j+1} - \alpha)u_x^+(\alpha) + \frac{1}{2}(x_{j+1} - \alpha)^2 u_{xx}^+(\alpha) + O(h^3).$$

Using the jump relation (2.4), the expression above can be written as

$$u(x_{j+1}) = u^-(\alpha) + (x_{j+1} - \alpha) \left(\frac{\beta^-}{\beta^+} u_x^-(\alpha) + \frac{C}{\beta^+} \right) + \frac{1}{2}(x_{j+1} - \alpha)^2 \frac{\beta^-}{\beta^+} u_{xx}^-(\alpha) + O(h^3).$$

The Taylor expansions of $u(x_{j-1})$ and $u(x_j)$ at α have the following expression

$$u(x_l) = u^-(\alpha) + (x_l - \alpha)u_x^-(\alpha) + \frac{1}{2}(x_l - \alpha)^2 u_{xx}^-(\alpha) + O(h^3), \quad l = j-1, j.$$

Therefore we have the following

$$\begin{aligned} & \gamma_{j,1}u(x_{j-1}) + \gamma_{j,2}u(x_j) + \gamma_{j,3}u(x_{j+1}) = (\gamma_{j,1} + \gamma_{j,2} + \gamma_{j,3})u^-(\alpha) \\ & + \left((x_{j-1} - \alpha)\gamma_{j,1} + (x_j - \alpha)\gamma_{j,2} + \frac{\beta^-}{\beta^+}(x_{j+1} - \alpha)\gamma_{j,3} \right) u_x^-(\alpha) + \gamma_{j,3}(x_{j+1} - \alpha) \frac{C}{\beta^+} \\ & + \frac{1}{2} \left((x_{j-1} - \alpha)^2\gamma_{j,1} + (x_j - \alpha)^2\gamma_{j,2} + \frac{\beta^-}{\beta^+}(x_{j+1} - \alpha)^2 \right) u_{xx}^-(\alpha) + O(\max_l |\gamma_{j,l}| h^3), \end{aligned}$$

after the Taylor expansions and collecting terms for $u^-(\alpha)$, $u_x^-(\alpha)$ and $u_{xx}^-(\alpha)$.

By matching the finite difference approximation with the differential equation at α from the $-$ side¹, we get the system of equations for the coefficients γ_j 's below:

$$\begin{aligned} & \gamma_{j,1} + \gamma_{j,2} + \gamma_{j,3} & = 0 \\ (2.9) \quad & -(\alpha - x_{j-1})\gamma_{j,1} - (\alpha - x_j)\gamma_{j,2} + \frac{\beta^-}{\beta^+}(x_{j+1} - \alpha)\gamma_{j,3} & = 0 \\ & \frac{1}{2}(\alpha - x_{j-1})^2\gamma_{j,1} + \frac{1}{2}(\alpha - x_j)^2\gamma_{j,2} + \frac{\beta^-}{2\beta^+}(x_{j+1} - \alpha)^2\gamma_{j,3} & = \beta^-. \end{aligned}$$

It is easy to verify that the γ 's in the left column of (2.7) satisfy the system above. Once those γ 's have been computed, it is easy to set the correction term C_j to match the remaining leading terms of the differential equation.

2.4. The IIM for general 1D elliptic interface problems

For a general interface problem in which all the coefficients $\beta(x)$, $\kappa(x)$, and $f(x)$, can have a finite jump at $x = \alpha$, and the solution itself can have a jump $[u] = \hat{C}$, in addition to the flux jump condition, $[\beta u_x] = C$, the IIM has been developed in [39]. The finite difference scheme at $x = x_j$ is the solution of the following linear system

$$\begin{aligned} & \gamma_{j,1} + \gamma_{j,2} + \left(1 + \frac{(x_{j+1} - \alpha)^2}{2\beta^+} [\kappa] \right) \gamma_{j,3} & = 0 \\ & (x_{j-1} - \alpha)\gamma_{j,1} + (x_j - \alpha)\gamma_{j,2} \\ (2.10) \quad & + \left\{ \frac{\beta^-}{\beta^+}(x_{j+1} - \alpha) + \left(\frac{\beta_x^-}{\beta^+} - \frac{\beta^- \beta_x^+}{(\beta^+)^2} \right) \frac{(x_{j+1} - \alpha)^2}{2} \right\} \gamma_{j,3} & = \beta_x^- \\ & \frac{(x_{j-1} - \alpha)^2}{2}\gamma_{j,1} + \frac{(x_j - \alpha)^2}{2}\gamma_{j,2} + \frac{(x_{j+1} - \alpha)^2 \beta^-}{2\beta^+} \gamma_{j,3} & = \beta^-. \end{aligned}$$

¹It is also possible to further expand at $x = x_j$ to match the differential equation at $x = x_j$. The order of convergence will be the same.

The correction term at $x = x_j$ is

(2.11)

$$C_j = \gamma_{j,3} \left\{ \hat{C} + (x_{j+1} - \alpha) \frac{C}{\beta^+} - \frac{(x_{j+1} - \alpha)^2}{2} \left(\frac{\beta_x^+ C}{(\beta^+)^2} - \kappa^+ \frac{\hat{C}}{\beta^+} - \frac{[f]}{\beta^+} \right) \right\}.$$

The linear system of equations for the coefficients of the finite difference equation at $x = x_{j+1}$, and the correction term C_{j+1} can be found in [39].

FIG. 2.1. Comparison of the computed solutions. The solid line is the exact solution. The ‘*’ is the result from the IIM which is exact. The ‘o’ is the result obtained from the smoothing method (1.5) with $\epsilon = 2h$ combined with the discrete cosine delta function. The mesh size is $h = 1/40$.

2.5. A numerical example of comparison

In Fig. 2.1, we show a comparison of the numerical results obtained from the IIM and the smoothing method with the discrete cosine delta function for 1D interface problem (2.1) with $\kappa = 0$. The source term is $f(x) = \delta(x - \alpha)$. The boundary condition is $u(0) = u(1) = 0$. It is easy to check that the exact solution is

$$u(x) = \begin{cases} Bx(1 - \alpha), & \text{if } 0 \leq x \leq \alpha, \\ B\alpha(1 - x), & \text{if } \alpha < x \leq 1, \end{cases}$$

where $B = -\frac{1}{\beta^+\alpha + \beta^-(1-\alpha)}$. The parameters are $\alpha = 1/3$, $\beta^- = 1$, $\beta^+ = 100$. In this case, the IIM gives the exact solution while the result (little ‘o’s’) computed from the smoothing method (1.5) with $\epsilon = 2h$ combined with the cosine discrete delta function (1.9) is obviously first order accurate.

3. THE IMMERSSED INTERFACE METHOD FOR TWO DIMENSIONAL PROBLEMS

In two space dimensions, an interface is a curve that we assume to be smooth. For an elliptic interface problem (1.3), the two jump conditions generally are

$$(3.1) \quad [u] \Big|_{\Gamma} = w(s), \quad [\beta u_n] \Big|_{\Gamma} = v(s),$$

where $w(s)$ and $v(s)$ are two functions defined only along the interface Γ , s is the arc-length of the interface, $u_n = \frac{\partial u}{\partial \mathbf{n}} = \nabla u \cdot \mathbf{n}$ is the normal derivative, and \mathbf{n} is the unit normal direction, see Fig. 3.1(a) for an illustration. The original IIM for two dimensional problems are proposed in [36, 39]. In the original IIM, a six-point

FIG. (a) A diagram of a rectangular domain $\Omega = \Omega^+ \cup \Omega^-$ with an immersed interface Γ . The coefficients such as $\beta(\mathbf{x})$ etc. may have a jump across the interface. (b) A diagram of the local coordinates in the normal and tangential directions, θ is the angle between the x -axis and the normal direction.

stencil is used at an irregular grid point. In [44], a new version of the IIM, the maximum principle preserving scheme, is proposed. Using the discrete maximum principle, the convergence of the IIM has been proved by constructing a comparison function. Before we explain the IIM for two dimensional problems, we first provide some theoretical preparations.

3.1. The local coordinates in the normal and tangential directions

Let (x^*, y^*) be a point on the interface Γ , it is more convenient to use the local coordinates in the normal and tangential directions:

$$(3.2) \quad \begin{aligned} \xi &= (x - x^*) \cos \theta + (y - y^*) \sin \theta, \\ \eta &= -(x - x^*) \sin \theta + (y - y^*) \cos \theta, \end{aligned}$$

where θ is the angle between the x -axis and the normal direction, pointing to the direction of a specified side.

In the neighborhood of (x^*, y^*) , the interface Γ can be parameterized as

$$(3.3) \quad \xi = \chi(\eta), \quad \text{with} \quad \chi(0) = 0, \quad \chi'(0) = 0.$$

The curvature of the interface at (x^*, y^*) then is $\chi''(0)$.

3.2. The interface relations

To derive the finite difference scheme at irregular grid points, we need to use the interface relations so that we can express the quantities from one side in terms of those from the other. The derivation is based on the original

jump conditions (3.1), their derivatives along the interface, and the partial differential equation itself. These relations are list below, see [36, 39] for the derivation,

$$\begin{aligned}
(3.4) \quad & u^+ = u^- + w, \quad u_\xi^+ = \rho u_\xi^- + \frac{v}{\beta^+}, \quad u_\eta^+ = u_\eta^- + w', \\
& u_{\xi\xi}^+ = \left(\frac{\beta_\xi^-}{\beta^+} - \chi'' \right) u_\xi^- + \left(\chi'' - \frac{\beta_\xi^+}{\beta^+} \right) u_\xi^+ + \frac{\beta_\eta^-}{\beta^+} u_\eta^- - \frac{\beta_\eta^+}{\beta^+} u_\eta^+ \\
& \quad + (\rho - 1) u_{\eta\eta}^- + \rho u_{\xi\xi}^- - w'' + \frac{[f]}{\beta^+} + \frac{[\kappa] u^- + \kappa^+ [u]}{\beta^+}, \\
& u_{\eta\eta}^+ = u_{\eta\eta}^- + (u_\xi^- - u_\xi^+) \chi'' + w'', \\
& u_{\xi\eta}^+ = \frac{\beta_\eta^-}{\beta^+} u_\xi^- - \frac{\beta_\eta^+}{\beta^+} u_\xi^+ + (u_\eta^+ - \rho u_\eta^-) \chi'' + \rho u_{\xi\eta}^- + \frac{v'}{\beta^+},
\end{aligned}$$

where $\rho = \beta^-/\beta^+$. These interface relations are used in deriving the finite difference equation.

3.3. An outline of the maximum principle preserving IIM

We assume the domain Ω is a rectangle, say $[a, b] \times [c, d]$. The IIM can be outline below.

- Generate a Cartesian grid

$$x_i = a + ih_x, \quad y_j = a + jh_y, \quad i = 0, 1, \dots, m, \quad j = 0, 1, \dots, n,$$

where $h_x = (b - a)/m$ and $h_y = (d - c)/n$. We say (x_i, y_j) is a *regular* grid point if (x_{i-1}, y_j) , (x_{i+1}, y_j) , (x_i, y_{j-1}) , and (x_i, y_{j+1}) are all on the same side of the interface as (x_i, y_j) is. Otherwise the grid point is called *irregular*, see Sec. 5.1 for more information.

- Use the standard finite difference equation at regular grid points. For example, at a regular grid point (x_i, y_j) , the FD equation is

$$\begin{aligned}
(3.5) \quad & \frac{\beta_{i+\frac{1}{2},j} u_{i+1,j} + \beta_{i-\frac{1}{2},j} u_{i-1,j} - (\beta_{i+\frac{1}{2},j} + \beta_{i-\frac{1}{2},j}) u_{ij}}{(h_x)^2} - \kappa u_{ij} \\
& + \frac{\beta_{i,j+\frac{1}{2}} u_{i,j+1} + \beta_{i,j-\frac{1}{2}} u_{i,j-1} - (\beta_{i,j+\frac{1}{2}} + \beta_{i,j-\frac{1}{2}}) u_{ij}}{(h_y)^2} = f_{ij}.
\end{aligned}$$

The local truncation error at regular grid points is $O(h^2)$, where $h = \max\{h_x, h_y\}$.

- If (x_i, y_j) is an irregular grid point, we use the method of undetermined coefficients

$$(3.6) \quad \sum_{k=1}^{n_s} \gamma_k U_{i+i_k, j+j_k} - \kappa_{ij} U_{ij} = f_{ij} + C_{ij}$$

to determine the coefficients γ_k 's of the finite difference equation and the correction term, where n_s is the number of grid points in the finite difference stencil. We usually take $n_s = 9$. The sum over k involves a finite number of points neighboring (x_i, y_j) . So each i_k, j_k will take values in the set $\{0, \pm 1, \pm 2, \dots\}$. The coefficients γ_k and the indices i_k, j_k should depend on (i, j) , but for simplicity of notation we drop the dependence in the notation.

- Use a linear solver, for example, a multigrid method such as the structured multigrid solver MGD9V [14], or an algebraic multigrid solver (AMG) [68] or the new multigrid solver in [1], to solve the system of the finite difference equations.

3.4. Set-up the system of equations for the coefficients of the FD scheme at an irregular grid point

At an irregular grid point $\mathbf{x}_{ij} = (x_i, y_j)$, we want to determine the coefficients of the finite difference equation in such a way that the local truncation error

$$(3.7) \quad T_{ij} = \sum_{k=1}^{n_s} \gamma_k u(x_{i+i_k}, y_{j+j_k}) - \kappa_{ij} u(x_i, y_j) - f(x_i, y_j) - C_{ij},$$

is as small as possible in the magnitude.

Using the immersed interface method, we choose a point $\mathbf{x}_{ij}^* = (x_i^*, y_j^*)$ on the interface Γ near (x_i, y_j) . Usually, we take \mathbf{x}_{ij}^* either as the orthogonal projection (explained in Sec. 5.2) of \mathbf{x}_{ij} on the interface or the intersection of the interface and one of axes. We use the Taylor expansion at \mathbf{x}_{ij}^* so that (3.6) matches the partial differential equation (1.3) up to second derivatives at \mathbf{x}_{ij}^* from a particular side of the interface, say the $-$ side. This will guarantee the consistency of the finite difference scheme. The Taylor expansion of each $u(x_{i+i_k}, y_{j+j_k})$ at \mathbf{x}_{ij}^* can be written as:

$$\begin{aligned} u(x_{i+i_k}, y_{j+j_k}) &= u(\xi_k, \eta_k) \\ &= u^\pm + \xi_k u_\xi^\pm + \eta_k u_\eta^\pm + \frac{1}{2} \xi_k^2 u_{\xi\xi}^\pm + \xi_k \eta_k u_{\xi\eta}^\pm + \frac{1}{2} \eta_k^2 u_{\eta\eta}^\pm + O(h^3), \end{aligned}$$

where the + or – superscript depends on whether (ξ_k, η_k) lies on the + or – side of Γ . Therefore the local truncation error T_{ij} can be expressed as a linear combination of the values $u^\pm, u_\xi^\pm, u_\eta^\pm, u_{\xi\xi}^\pm, u_{\xi\eta}^\pm, u_{\eta\eta}^\pm$

$$(3.8) \quad \begin{aligned} T_{ij} = & a_1 u^- + a_2 u^+ + a_3 u_\xi^- + a_4 u_\xi^+ + a_5 u_\eta^- + a_6 u_\eta^+ + a_7 u_{\xi\xi}^- \\ & + a_8 u_{\xi\xi}^+ + a_9 u_{\eta\eta}^- + a_{10} u_{\eta\eta}^+ + a_{11} u_{\xi\eta}^- + a_{12} u_{\xi\eta}^+ - \kappa^- u^- \\ & - f^- - C_{ij} + O(\max_k |\gamma_k| h^3). \end{aligned}$$

The coefficients a_l depend only on the position of the stencil relative to the interface. They are independent of the functions u, κ and f . If we define the index sets K^+ and K^- by

$$K^\pm = \{k : (\xi_k, \eta_k) \text{ is on the } \pm \text{ side of } \Gamma\},$$

then the a_{2j-1} terms are given by

$$(3.9) \quad \begin{aligned} a_1 &= \sum_{k \in K^-} \gamma_k, & a_3 &= \sum_{k \in K^-} \xi_k \gamma_k, & a_5 &= \sum_{k \in K^-} \eta_k \gamma_k, \\ a_7 &= \frac{1}{2} \sum_{k \in K^-} \xi_k^2 \gamma_k, & a_9 &= \frac{1}{2} \sum_{k \in K^-} \eta_k^2 \gamma_k, & a_{11} &= \sum_{k \in K^-} \xi_k \eta_k \gamma_k. \end{aligned}$$

The a_{2j} terms have the same expressions as a_{2j-1} except the summation is taken over K^+ .

Using the interface relations (3.4), we eliminate the quantities of one particular side, say, the + side, in (3.8) in terms of those from the other side, say, the – side, and collect terms to get an expression below

$$(3.10) \quad \begin{aligned} T_{ij} = & \left(a_1 + \frac{a_8 [\kappa]}{\beta^+} + a_2 \right) u^- + \left\{ a_3 + a_8 \left(\frac{\beta_\xi^-}{\beta^+} - \chi'' \right) + a_{10} \chi'' + a_{12} \frac{\beta_\eta^-}{\beta^+} \right. \\ & \left. + \rho \left(a_4 + a_8 \left(\chi'' - \frac{\beta_\xi^+}{\beta^+} \right) - a_{10} \chi'' - a_{12} \frac{\beta_\eta^+}{\beta^+} \right) - \beta_\xi^- \right\} u_\xi^- \\ & + \left\{ a_5 + a_6 + a_8 \left(\frac{\beta_\eta^-}{\beta^+} - \frac{\beta_\eta^+}{\beta^+} \right) + a_{12} (1 - \rho) \chi'' - \beta_\eta^- \right\} u_\eta^- \\ & + \{ a_7 + a_8 \rho - \beta^- \} u_{\xi\xi}^- + \{ a_9 + a_{10} + a_8 (\rho - 1) - \beta^- \} u_{\eta\eta}^- \\ & + \{ a_{11} + a_{12} \rho \} u_{\xi\eta}^- - \kappa^- u^- - f^- + (\hat{T}_{ij} - C_{ij}) + O(h), \end{aligned}$$

where

$$\begin{aligned}
(3.11) \quad \hat{T}_{ij} = & a_2 w + a_{12} \frac{v'}{\beta^+} + \left(a_6 - \frac{a_8 \beta_\xi^+}{\beta^+} + a_{12} \chi'' \right) w' \\
& + a_{10} w'' + \frac{1}{\beta^+} \left(a_4 + a_8 \left(\chi'' - \frac{\beta_\xi^+}{\beta^+} \right) - a_{10} \chi'' - a_{12} \frac{\beta_\eta^+}{\beta^+} \right) v \\
& + a_8 \left\{ \frac{[f]}{\beta^+} + \frac{\kappa^+ w}{\beta^+} - w'' \right\}.
\end{aligned}$$

We want to make the magnitude of the truncation error as small as possible by choosing γ_k 's so that the coefficients of u^- , u_ξ^- , u_η^- , \dots vanish. Therefore we set the linear system of equations for the coefficients as

$$\begin{aligned}
(3.12) \quad & a_1 + a_2 + a_8 \frac{[\kappa]}{\beta^+} = 0 \\
& a_3 + \rho a_4 + a_8 \frac{\beta_\xi^- - \rho \beta_\xi^+ - [\beta] \chi''}{\beta^+} + a_{10} \frac{[\beta] \chi''}{\beta^+} + a_{12} \frac{\beta_\eta^- - \rho \beta_\eta^+}{\beta^+} = \beta_\xi^- \\
& a_5 + a_6 - a_8 \frac{[\beta_\eta]}{\beta^+} + a_{12} (1 - \rho) \chi'' = \beta_\eta^- \\
& a_7 + a_8 \rho = \beta^- \\
& a_9 + a_{10} + a_8 (\rho - 1) = \beta^- \\
& a_{11} + a_{12} \rho = 0.
\end{aligned}$$

Once the γ_k 's are obtained, we set $C_{ij} = \hat{T}_{ij}$, which is given by (3.11). If we use a six-point stencil and (3.12) has a solution, then this leads to the original IIM [36].

3.5. Enforcing the maximum principle using an optimization approach

The stability of the finite difference equations is guaranteed by enforcing the sign constraint of the discrete maximum principle, see Morton and Mayers [57]. The sign restriction on the coefficients γ_k 's in (3.6) are

$$(3.13) \quad \gamma_k \geq 0 \quad \text{if} \quad (i_k, j_k) \neq (0, 0), \quad \gamma_k < 0 \quad \text{if} \quad (i_k, j_k) = (0, 0).$$

Note that at regular grid points, the standard central finite difference equations satisfy the sign constraints. We form the following constrained quadratic optimization problem whose solution is the coefficients of the finite difference

equation at the irregular grid point \mathbf{x}_{ij} :

$$(3.14) \quad \min_{\gamma} \left\{ \frac{1}{2} \|\gamma - g\|_2^2 \right\}, \quad \text{subject to}$$

$$A_{\gamma} = b, \quad \gamma_k \geq 0, \quad \text{if } (i_k, j_k) \neq (0, 0); \quad \gamma_k < 0, \quad \text{if } (i_k, j_k) = (0, 0),$$

where $\gamma = [\gamma_1, \gamma_2, \dots, \gamma_{n_s}]^T$ is the vector composed of the coefficients of the finite difference equation; $A_{\gamma} = b$ is the system of linear equations (3.12); and $g \in R^{n_s}$ has the following components: $g \in R^{n_s}$,

$$(3.15) \quad g_k = \frac{\beta_{i+i_k, j+j_k}}{h^2}, \quad \text{if } (i_k, j_k) \in \{(-1, 0), (1, 0), (0, -1), (0, 1)\};$$

$$g_k = -\frac{4\beta_{i, j}}{h^2}, \quad \text{if } (i_k, j_k) = (0, 0); \quad g_k = 0, \quad \text{Otherwise.}$$

If $[\beta] = 0$, then the solution to the optimization problem is the coefficients of the standard central FD equation using the five-point stencil. The existence of the solution to the optimization problem has been proved in [44]. We use the **QL** program developed by K. Schittkowski [71] to solve the quadratic optimization problem. The coefficient matrix of the finite difference approximation to the PDE from the maximum preserving scheme is an M-matrix which guarantees convergence of the multigrid methods that we used. The additional cost in constructing the finite difference equations at irregular grid points is usually less than 5% of the total CPU time. We refer the readers to [44] for the detailed analysis and numerical examples.

4. THE FAST IMMERSSED INTERFACE METHOD FOR INTERFACE PROBLEMS WITH PIECEWISE CONSTANT BUT DISCONTINUOUS COEFFICIENT

For many application problems, the coefficient in the elliptic equation (1.3) is piecewise constant. For example, it is reasonable to assume that the density and viscosity are constants in each phase for a multi-phase flow problem. In [42], a fast IIM method is proposed for this type of interface problems. One of remarkable properties of the fast IIM for the interface problems is that the number of iterations is independent of both the mesh size and the jump in β . And with minor modifications, the method can be used for solving Poisson equations on general domains, which have been applied to many applications [15, 16, 19, 51, 22].

In this section, we briefly discuss the fast IIM for interface problems (1.3), (3.1) with piecewise constant coefficient β and $\kappa \equiv 0$. Divided by the coefficient in each sub-domain of Ω , the original problem (1.3) can be written as

$$(4.1) \quad \Delta u = \frac{f}{\beta}, \quad \text{if } \mathbf{x} \in \Omega^+ \cup \Omega^- - \Gamma,$$

along with the jump conditions (3.1) and the boundary condition on $\partial\Omega$. The Poisson equation above is only valid in the interior of the domain excluding the interface Γ .

As we mentioned earlier in Sec. 3.5, for a Poisson equation with jumps $[u] = w$ and $[u_n] = v$, the finite difference equations using the IIM are the standard central five-point discrete Laplacian plus correction terms at irregular grid points. The resulting linear system of equations can be solved with one call to a fast Poisson solver. However, if $[\beta] \neq 0$, the second jump condition is in the flux $[\beta u_n] = v$ instead of $[u_n] = v$. We can not divide β from the flux jump condition $[\beta u_n] = v$ because β is discontinuous. As described in [42], the idea of the fast IIM is to augment an unknown $[u_n] = g$ to have the following system

$$(4.2) \quad \begin{aligned} \Delta u &= \frac{f}{\beta}, \quad \text{if } \mathbf{x} \in \Omega^+ \cup \Omega^- - \Gamma, \\ [u] &= w, \quad [\beta u_n] = v, \quad [u_n] = g. \end{aligned}$$

Note that g is also an unknown. The system is still closed because of an additional equation $[u_n] = g$.

In the discretization, we represent the unknown jump $g = [u_n]$ only at certain projections \mathbf{x}_l^* ($l = 1, 2, \dots$) of irregular grid points from a particular side of the interface. So now there are two steps discretizations:

- The system of the finite difference equations, which is obtained from the IIM with given jumps $[u] = w$ and $[u_n] = g$, can be written as (in the matrix-vector form)

$$(4.3) \quad AU + BG = F + F_w = F_1,$$

where U is the approximation to $u(\mathbf{x})$ at all grid points, G is a discrete form of $g(s)$ at the chosen points on the interface, A is the matrix obtained from the standard five point discrete Laplacian, F is the vector formed from the source term; F_w is the part of the correction terms corresponding to the jump $[u] = w$, and $-BG$ is the part of the correction terms corresponding to the jump $[u_n] = g$.

- The discretization of the flux jump condition $[\beta u_n] = v$ in terms of u , $[u] = w$, and $[u_n] = g$ using an interpolation scheme, can be written as

$$(4.4) \quad EU + DG = F_2,$$

where E, D , are two matrices.

If we put the two systems (4.3) and (4.4) together, we get

$$(4.5) \quad \begin{bmatrix} A & B \\ E & D \end{bmatrix} \begin{bmatrix} U \\ G \end{bmatrix} = \begin{bmatrix} F_1 \\ F_2 \end{bmatrix}.$$

Since the dimension of G , which is defined at a number of points on the interface, is much smaller than the dimension of U , which is defined at all grid points, it is advantageous to focus on the Schur complement

$$(4.6) \quad (D - EA^{-1}B)G = F_2 - EA^{-1}F_1$$

for the unknown G . The Schur complement system can be solved using the GMRES method [69]. Each iteration involves a call to a fast Poisson solver and an interpolation scheme of (4.4) for the flux jump condition $[\beta u_n] = v$ to get the residual vector. When the convergence criteria is met, we not only have an approximate solution to the PDE, but also the normal derivatives of the solution from each side of the interface, see [42].

In Table 4.1, we show a grid refinement analysis of the fast IIM with different jump in β . The interface is

$$\begin{cases} X = r(\theta) \cos \theta + x_c, \\ Y = r(\theta) \sin \theta + y_c, \end{cases} \quad r(\theta) = r_0 + 0.2 \sin(\omega \theta), \quad 0 \leq \theta < 2\pi.$$

We shifted the center of the interface from the origin to avoid any advantages of symmetry. The source term is

$$f(x, y) = \begin{cases} 4, & \text{if } \mathbf{x} \in \Omega^-, \\ 16r^2 & \text{if } \mathbf{x} \in \Omega^+, \end{cases}$$

where $r = \sqrt{x^2 + y^2}$. The exact solution is chosen as

$$u(x, y) = \begin{cases} \frac{r^2}{\beta^-}, & \text{if } (x, y) \in \Omega^-, \\ \frac{r^4 + C_0 \log(2r)}{\beta^+} + C_1 \left(\frac{r_0^2}{\beta^-} - \frac{r_0^4 + C_0 \log(2r_0)}{\beta^+} \right), & \text{if } (x, y) \in \Omega^+. \end{cases}$$

The jump conditions $[u]$ and $[\beta u_n]$ are obtained from the exact solution. In Table 4.1, E_1, E_2 , and E_3 , are the errors in the maximum norm for the solution u , the normal derivatives u_n^- , and u_n^+ respectively. For a second order method, the ratio r_i should approach number 4. In the last column of Table 4.1, k is the number of iterations of the GMRES iteration. We see clearly second order

accuracy for all the quantities, and the number of iterations is independent of both the mesh size n and the jump in β .

TABLE 4.1. A grid refinement analysis for the fast IIM. The parameters are $r_0 = 0.5$, $x_c = y_c = 0.2/\sqrt{20}$, $\omega = 5$, and $m = n_b = n$. The number of iterations of the GMRES iterations is independent of both the mesh size n and the jump in the coefficient β .

n	β^+	β^-	E_1	E_2	E_3	r_1	r_2	r_3	k
40	2	1	$2.285 \cdot 10^{-3}$	$2.23 \cdot 10^{-3}$	$7.434 \cdot 10^{-3}$				7
80	2	1	$5.225 \cdot 10^{-4}$	$5.956 \cdot 10^{-3}$	$1.987 \cdot 10^{-2}$	4.37	3.74	3.74	7
160	2	1	$1.269 \cdot 10^{-4}$	$1.827 \cdot 10^{-4}$	$6.101 \cdot 10^{-4}$	4.12	3.26	3.26	7
320	2	1	$2.988 \cdot 10^{-5}$	$5.038 \cdot 10^{-5}$	$1.678 \cdot 10^{-4}$	4.25	3.63	3.64	7

n	β^+	β^-	E_1	E_2	E_3	r_1	r_2	r_3	k
40	10000	1	$6.552 \cdot 10^{-5}$	$6.331 \cdot 10^{-4}$	$2.110 \cdot 10^{-4}$				8
80	10000	1	$7.847 \cdot 10^{-6}$	$8.366 \cdot 10^{-5}$	$2.785 \cdot 10^{-5}$	8.35	7.57	7.58	8
160	10000	1	$5.988 \cdot 10^{-7}$	$9.192 \cdot 10^{-7}$	$3.033 \cdot 10^{-6}$	13.1	9.10	9.18	8
320	10000	1	$5.859 \cdot 10^{-8}$	$2.058 \cdot 10^{-7}$	$6.887 \cdot 10^{-7}$	10.2	4.47	4.40	7

4.1. An application of the fast IIM for Helmholtz/Poisson equations on irregular domains

The idea of the fast interface IIM described in the previous section can be used with a little modifications to solve Helmholtz/Poisson equations of the form

$$(4.7) \quad \begin{aligned} \Delta u - \lambda u &= f(\mathbf{x}), \quad \mathbf{x} \in \Omega, \\ q(u, u_n) &= 0, \quad \mathbf{x} \in \partial\Omega, \end{aligned}$$

defined on an irregular domain Ω (interior or exterior), where $q(u, u_n)$ is a prescribed linear boundary condition along the boundary $\partial\Omega$. We will demon-

strate the idea for interior problems with a Dirichlet boundary condition $u|_{\partial\Omega} = u_0(\mathbf{x})$.

We embed Ω into a cube R and extend the PDE and the source term to the entire cube R

$$(4.8) \quad \Delta u - \lambda u = \begin{cases} f, & \text{if } \mathbf{x} \in \Omega, \\ 0, & \text{if } \mathbf{x} \in R - \Omega, \end{cases} \quad u|_{\partial\Omega} = u_0(\mathbf{x}),$$

$$\begin{cases} [u] = g, & \text{on } \partial\Omega, \\ [u_n] = 0, & \text{on } \partial\Omega, \\ u = 0, & \text{on } \partial R, \end{cases} \quad \text{or} \quad \begin{cases} [u] = 0, & \text{on } \partial\Omega, \\ [u_n] = g, & \text{on } \partial\Omega, \\ u = 0, & \text{on } \partial R. \end{cases}$$

Again, the solution u is a functional of g . We determine $g(s)$ such that the solution $u(g)$ satisfies the boundary condition $u(g)|_{\partial\Omega} = u_0(\mathbf{x})$. This can be solved using the GMRES iteration exactly as we discussed earlier. The only difference is the way in computing the residual vector.

There are other fast elliptic solvers for elliptic PDEs defined on irregular domains using embedding or fictitious domain techniques. The earlier ones include the capacitance matrix method [66], the integral equation approach [55, 56], and the recent finite volume method [24].

In [83], an immersed interface method for boundary value problems (IIMB) on irregular domains is developed, particularly for Dirichlet boundary conditions. It was shown in [83] that the IIMB method is second order accurate in the maximum norm and the Schur complement system is well-conditioned. The IIMB method was applied to underground water simulations using the stream-vorticity function in [83].

Forgelson and Keener [18] have developed an embedding method for Laplacian equations on irregular domains with a Neumann boundary condition in two and three dimensions. With careful selection of the stencils, the method is second order accurate and produces a matrix that is stable (diagonally semi-dominant). Dumett and Keener [17] have also extended the embedding method to anisotropic elliptic boundary value problems on irregular domains in two space dimensions when $\beta(\mathbf{x})$ in (1.3) is an anisotropic matrix.

5. SOME IMPLEMENTATION DETAILS OF THE IIM

5.1. Interface expressions

To solve an interface problem numerically, we need the information of the interface such as the tangential and normal directions, the curvature etc. We list some common approaches used to express interfaces below.

- **Analytic expressions.** If the interface is fixed, we may have an analytic expression for the interface, see for example [40]. However, it usually does not work for moving interface and free boundary problems.

- **The Lagrangian formulation.** This approach is also called the particle method. In this approach, a number of control points on the interface, say \mathbf{X}_k , $k = 1, 2, \dots$, are given. Other interface information such as the normal and the tangential derivatives, the curvature etc., can be obtained from those control points. In [39], a cubic spline interpolation package was developed for a closed interface in 2D. The package can be used to compute the arc-length, the first and second tangential derivatives of any given function defined on the interface.

- **The level set method, an Eulerian approach.** In this approach, the interface is the zero level set of a Lipschitz continuous function $\varphi(\mathbf{x})$ defined on the entire domain. For example, if the interface is the unit circle in 2D, then one choice of a level set function is $\varphi(x, y) = \sqrt{x^2 + y^2} - 1$. For a general interface, the level set function is often chosen as the signed distance function.

Note that with a level set function, the interface is explicitly defined by a grid function $\varphi_{ij} = \varphi(x_i, y_j)$ in 2D. The unit normal direction is simply $\nabla\varphi/|\nabla\varphi|$, and the curvature is $\nabla \cdot \frac{\nabla\varphi}{|\nabla\varphi|}$. All these information can be calculated using the central finite difference schemes at grid points. For a non-grid point, the information can be computed in terms of the information at the four neighboring grid points using the bi-linear interpolation, see [19].

If the interface is expressed as the zero level set of a function φ_{ij} , then it is easy to classify a grid point as regular or irregular for elliptic interface problems. Let (x_i, y_j) be a grid point, define

$$(5.1) \quad \begin{aligned} \varphi_{i,j}^{max} &= \max\{\varphi_{i-1,j}, \varphi_{i,j}, \varphi_{i+1,j}, \varphi_{i,j-1}, \varphi_{i,j+1}\}, \\ \varphi_{i,j}^{min} &= \min\{\varphi_{i-1,j}, \varphi_{i,j}, \varphi_{i+1,j}, \varphi_{i,j-1}, \varphi_{i,j+1}\}. \end{aligned}$$

We call (x_i, y_j) an **irregular grid point** if $\varphi_{i,j}^{max} \varphi_{i,j}^{min} \leq 0$. Otherwise the grid point is a regular one.

5.2. Finding the orthogonal projection of an irregular grid point on the interface

Using the IIM, we often need to find a point \mathbf{x}^* on the interface near an irregular grid point, say \mathbf{x} . If the interface is expressed as the zero level set of a function $\varphi(\mathbf{x})$ that is twice differentiable in the neighborhood of the interface, then we can easily find an accurate approximation of the orthogonal projection

of the irregular grid point on the interface using

$$(5.2) \quad \mathbf{x}^* = \mathbf{x} + \alpha \mathbf{p}, \quad \mathbf{p} = \frac{\nabla \varphi}{|\nabla \varphi|},$$

where α is determined from the quadratic equation below:

$$(5.3) \quad \varphi(\mathbf{x}) + |\nabla \varphi| \alpha + \frac{1}{2} (\mathbf{p}^T \text{He}(\varphi) \mathbf{p}) \alpha^2 = 0,$$

and $\text{He}(\varphi)$ is the Hessian matrix of φ . The projection computed using this procedure has third order accuracy. Note that the formula is valid in both two and three dimensions.

5.3. Some issues for three dimensional problems

The IIM developed for 3D problems in [39, 40] assumes an analytic expression of the interface. Recently, the maximum principle preserving IIM and the fast IIM for interface problems with piecewise constant coefficient have been developed in [15] for three dimensional problems in which the interface is expressed in terms of a level set function. While the main ideas are similar, the implementation and derivation may be substantial different. We mention below some crucial components of the IIM for three dimensional problems.

• **The local coordinates transformation and the choice of the tangential directions.** Given a point (x^*, y^*, z^*) on the interface Γ , let $\boldsymbol{\xi}$ be the normal direction of Γ , and $\boldsymbol{\eta}, \boldsymbol{\tau}$, be two orthogonal directions tangential to Γ , then the local coordinates transformation is given by

$$(5.4) \quad \begin{pmatrix} \xi \\ \eta \\ \tau \end{pmatrix} = A \begin{pmatrix} x - x^* \\ y - y^* \\ z - z^* \end{pmatrix}, \quad A = \begin{pmatrix} \alpha_{x\xi} & \alpha_{y\xi} & \alpha_{z\xi} \\ \alpha_{x\eta} & \alpha_{y\eta} & \alpha_{z\eta} \\ \alpha_{x\tau} & \alpha_{y\tau} & \alpha_{z\tau} \end{pmatrix},$$

where $\alpha_{x\xi}$ represents the directional cosine between the x -axis and $\boldsymbol{\xi}$, and so forth. For any differentiable function $p(x, y, z)$, we have

$$(5.5) \quad \begin{pmatrix} \bar{p}_\xi \\ \bar{p}_\eta \\ \bar{p}_\tau \end{pmatrix} = A \begin{pmatrix} p_x \\ p_y \\ p_z \end{pmatrix},$$

where $\bar{p}(\xi, \eta, \tau) = p(x, y, z)$, and

$$(5.6) \quad \begin{pmatrix} \bar{p}_{\xi\xi} & \bar{p}_{\xi\eta} & \bar{p}_{\xi\tau} \\ \bar{p}_{\eta\xi} & \bar{p}_{\eta\eta} & \bar{p}_{\eta\tau} \\ \bar{p}_{\tau\xi} & \bar{p}_{\tau\eta} & \bar{p}_{\tau\tau} \end{pmatrix} = A \begin{pmatrix} p_{xx} & p_{xy} & p_{xz} \\ p_{yx} & p_{yy} & p_{yz} \\ p_{zx} & p_{zy} & p_{zz} \end{pmatrix} A^T,$$

where A^T is the transpose of A . It is easy to verify that $A^T A = I$, where I is the identity matrix.

If the interface is expressed as the zero level set of a function $\varphi(x, y, z)$, then the normal direction $\boldsymbol{\xi}$, the two tangential directions $\boldsymbol{\eta}$ and $\boldsymbol{\tau}$ can be selected as

$$(5.7) \quad \boldsymbol{\xi} = \frac{\nabla\varphi}{|\nabla\varphi|} = (\varphi_x, \varphi_y, \varphi_z)^T / \sqrt{\varphi_x^2 + \varphi_y^2 + \varphi_z^2},$$

$$(5.8) \quad \boldsymbol{\eta} = (\varphi_y, -\varphi_x, 0)^T / \sqrt{\varphi_x^2 + \varphi_y^2},$$

if $\varphi_x^2 + \varphi_y^2 \neq 0$. Otherwise we choose

$$(5.9) \quad \boldsymbol{\eta} = (\varphi_z, 0, -\varphi_x)^T / \sqrt{\varphi_x^2 + \varphi_z^2}.$$

The corresponding second tangential direction is

$$(5.10) \quad \boldsymbol{\tau} = \frac{\boldsymbol{\xi} \times \boldsymbol{\eta}}{|\boldsymbol{\xi} \times \boldsymbol{\eta}|} = \frac{\mathbf{s}}{|\mathbf{s}|}, \quad \text{where } \mathbf{s} = (\varphi_x\varphi_z, \varphi_y\varphi_z, -\varphi_x^2 - \varphi_y^2)^T,$$

if $\varphi_x^2 + \varphi_y^2 \neq 0$. Otherwise we choose

$$(5.11) \quad \boldsymbol{\tau} = \frac{\mathbf{t}}{|\mathbf{t}|}, \quad \text{where } \mathbf{t} = (-\varphi_x\varphi_y, \varphi_x^2 + \varphi_z^2, -\varphi_y\varphi_z)^T.$$

5.4. Related software packages

Several packages (collections of Fortran subroutines) have been developed and are available to the public through anonymous ftp ². The interface (closed surfaces within the solution domain) can be expressed as a set of ordered points (Lagrangian formulation) or a level set function (Eulerian formulation). We briefly describe the packages available and choices of the packages.

- It is recommended that the maximum principle preserving IIM be used for self-adjoint elliptic interface problems with variable and discontinuous coefficient, for example, non-linear interface problems whose coefficient depending on the solution.
- For self-adjoint elliptic interface problems with piecewise constant coefficient, the fast IIM method is recommended.

² ftp.ncsu.edu under the directory /pub/math/zhilin/Packages.

- Packages for Poisson or Helmholtz equations on irregular domains, either interior or exterior, are available. The boundary (can be multi-connected) of the domain should be expressed in terms of a level set function. Like other elliptic solvers, the method may not work very well for Helmholtz equations that behave like hyperbolic equations.

6. THE IMMERSED INTERFACE METHOD IN POLAR COORDINATES

Polar, cylindrical, and spherical coordinates are widely used for many applications especially in electro-magnetics, and problems with an infinite domain. The IIM developed for Cartesian grids can not be applied directly for polar coordinates because the jump relations of the solution and its derivatives are not as useful and informative in polar coordinates as those derived in [36, 39] for Cartesian coordinates.

In [50], the authors have proposed a new formulation and a new algorithm for following elliptic interface problems

$$(6.1) \quad \Delta u = f, \quad \mathbf{x} \in \mathcal{R} - \Gamma, \quad [u]_{\Gamma} = w(s), \quad [u_n]_{\Gamma} = v(s),$$

with a prescribed boundary condition along $r = r_{max}$, where \mathcal{R} is a circular domain $0 \leq r \leq r_{max}$, and $\Gamma \in \mathcal{R}$ is an interface. We assume that $w \in C^2(\Gamma)$ and $v \in C^2(\Gamma)$.

In the neighborhood of the interface Γ , which is the zero level set $\varphi = 0$, we extend $w(\mathbf{X}(s))$ and $v(\mathbf{X}(s))$ along the normal line (both directions) using the formulae

$$(6.2) \quad w_e(\mathbf{x}) = w_e(\mathbf{X}(s) + \alpha \mathbf{n}) = w(\mathbf{X}(s)),$$

$$(6.3) \quad v_e(\mathbf{x}) = v_e(\mathbf{X}(s) + \alpha \mathbf{n}) = v(\mathbf{X}(s)),$$

for all $\alpha \in R$ such that the normal lines do not intersect. We then construct the following function based on the extensions

$$(6.4) \quad \tilde{u}(\mathbf{x}) = w_e(\mathbf{x}) + v_e(\mathbf{x}) \frac{\varphi(\mathbf{x})}{|\nabla \varphi(\mathbf{x})|}.$$

Note that $\tilde{u}(\mathbf{x}) \in C^2$ in the neighborhood of the interface Γ since we assume that $w(s)$, $v(s)$, and $\Gamma(s)$ are all in C^2 . Define also

$$(6.5) \quad \hat{u}(\mathbf{x}) = H(\varphi(\mathbf{x}))\tilde{u}(\mathbf{x}) = \begin{cases} 0, & \text{if } \varphi(\mathbf{x}) < 0, \\ \frac{1}{2}\tilde{u}(\mathbf{x}), & \text{if } \varphi(\mathbf{x}) = 0, \\ \tilde{u}(\mathbf{x}), & \text{if } \varphi(\mathbf{x}) > 0, \end{cases}$$

in the same neighborhood in which $\tilde{u}(\mathbf{x})$ is well defined. We have the following theorem.

Theorem 6.1. *Let $u(\mathbf{x})$ be the solution of (6.1), $\hat{u}(\mathbf{x})$ be defined in (6.5). Define $q(\mathbf{x}) = u(\mathbf{x}) - \hat{u}(\mathbf{x})$. Then in the neighborhood of the interface where $w_e(\mathbf{x})$ and $v_e(\mathbf{x})$ are well defined, $q(\mathbf{x})$ is the solution of the following problem*

$$(6.6) \quad \Delta q(\mathbf{x}) = f(\mathbf{x}) - H(\varphi(\mathbf{x})) \Delta \hat{u}(\mathbf{x}), \quad \mathbf{x} \in \mathcal{R} - \Gamma,$$

$$(6.7) \quad [q]_{\Gamma} = 0, \quad [q_{\tau}]_{\Gamma} = 0, \quad [q_n]_{\Gamma} = 0,$$

where $\boldsymbol{\tau}$ is the unit tangent direction. In other words, the new function $q(\mathbf{x})$ is a smooth function across the interface Γ .

The proof can be found in [50] and will be omitted here. Since $q(\mathbf{x})$ is smooth, we can use the standard finite difference scheme with minor modifications (to take care of the jump in the second order derivatives) to get an accurate $q(\mathbf{x})$, and then recover the solution $u(\mathbf{x})$ according to $u(\mathbf{x}) = q(\mathbf{x}) + \hat{u}(\mathbf{x})$. The fast solver for elliptic interface problems with piecewise constant coefficients based on the new formulation above has also been developed in polar coordinates and the method is similar to the discussions in Sec. 4. We refer the readers to [50] for the detailed algorithms and numerical results.

7. THE IMMERSSED INTERFACE METHOD USING FINITE ELEMENT FORMULATIONS

In the previous sections, we have been focused on finite difference methods for interface problems because they are usually simple to understand and implement. However, sometimes a finite element formulation is preferred because it is relatively easier to prove the convergence. Finite element methods have less regularity requirements for the coefficients, the source term, and the solution than finite difference methods do. In fact, the weak form for elliptic interface problems (1.3) is

$$(7.1) \quad \iint_{\Omega} \beta \nabla u \nabla \phi \, d\mathbf{x} + \iint_{\Omega} \kappa uv \, d\mathbf{x} = - \iint_{\Omega} f \phi \, d\mathbf{x} + \int_{\Gamma} v \phi \, ds, \quad \forall \phi(\mathbf{x}) \in H_0^1(\Omega),$$

which does allow the discontinuity in the coefficient β , we refer the readers to [45] for the derivation.

7.1. The modified basis functions for one dimensional problems

Unless the interface α in (2.1) itself is a node, the solution obtained from the standard finite element method using the linear basis functions is only first

order accurate in the maximum norm. In [43], modified basis functions which are defined below

$$(7.2) \quad \phi_i(x_k) = \begin{cases} 1, & \text{if } k = i, \\ 0, & \text{otherwise,} \end{cases}$$

$$(7.3) \quad [\phi_i] = 0, \quad [\beta\phi'_i] = 0,$$

were constructed. Obviously, if $x_j < \alpha < x_{j+1}$, then only ϕ_j and ϕ_{j+1} need to be changed to satisfy the second jump condition. Using the method of undetermined coefficients, we can conclude that

$$\phi_j(x) = \begin{cases} 0, & 0 \leq x < x_{j-1}, \\ \frac{x-x_{j-1}}{h}, & x_{j-1} \leq x < x_j, \\ \frac{x_j-x}{D} + 1, & x_j \leq x < \alpha, \\ \frac{\rho(x_{j+1}-x)}{D}, & \alpha \leq x < x_{j+1}, \\ 0, & x_{j+1} \leq x \leq 1, \end{cases} \quad \phi_{j+1}(x) = \begin{cases} 0, & 0 \leq x < x_j, \\ \frac{x-x_j}{D}, & x_j \leq x < \alpha, \\ \frac{\rho(x-x_{j+1})}{D} + 1, & \alpha \leq x < x_{j+1}, \\ \frac{x_{j+2}-x}{h}, & x_{j+1} \leq x \leq x_{j+2}, \\ 0, & x_{j+2} \leq x \leq 1. \end{cases}$$

where

$$\rho = \frac{\beta^-}{\beta^+}, \quad D = h - \frac{\beta^+ - \beta^-}{\beta^+} (x_{j+1} - \alpha).$$

Fig. 7.1 shows several plots of the modified basis functions $\phi_j(x)$, $\phi_{j+1}(x)$, and some neighboring basis functions, which are the standard hat functions. At the interface α , we can see clearly the kink in the basis function which reflect the natural jump condition.

Using the modified basis function, it has been shown in [43] that the finite element solution obtained from the Galerkin method with the new basis functions is second order accurate in the maximum norm.

FIG. 7.1. Plot of some basis function near the interface with different β^- and β^+ . The interface is at $\alpha = \frac{2}{3}$.

For 1D interface problems, the FD and FE methods discussed here are not very much different. The FE method likely perform better for self-adjoint problems, while the FD method is more flexible for general elliptic interface problems.

7.2. Modified basis functions for two dimensional problems

The similar idea above has been applied to two dimensional problems with a uniform Cartesian triangulation [45]. The piecewise linear basis function centered at a node is defined as:

$$(7.4) \quad \phi_i(\mathbf{x}_j) = \begin{cases} 1, & \text{if } i = j \\ 0, & \text{otherwise,} \end{cases} \quad [u]_{\Gamma} = 0, \quad \left[\beta \frac{\partial \phi_i}{\partial \mathbf{n}} \right]_{\Gamma} = 0, \quad \phi_i|_{\partial\Omega} = 0.$$

We call the space formed by all the basis function $\phi_i(\mathbf{x})$ as the immersed finite element space (IFE).

It is easy to show that the linear basis functions defined at a nodal point exists and it is unique. It has also been proved in [45] that for the solution of the interface problem (1.3), there is an interpolation function $u_I(\mathbf{x})$ in the IFE space that approximates $u(x)$ to second order accuracy in the maximum norm.

However, as we can see from Fig. 7.2(b), a linear basis function may be discontinuous along some edges. Therefore such IFE space is a non-conforming

finite element space. Theoretically, it is easy to prove the corresponding Galerkin finite

(a) (b)

FIG. (a) A standard domain of six triangles with an interface cutting through. (b) A global basis function on its support in the *non-conforming* immersed finite element space. The basis function has small jump across some edges.

element method is at least first order accurate, see [45]. In practice, it behaves much better than the standard finite element without any modifications. Numerically, the computed solution has super linear convergence.

A *conforming* IFE space is also proposed in [45]. The basis functions are still piecewise linear. The idea is to extend the support of the basis function along interface to one more triangle to keep the continuity. The conforming immersed finite element method is indeed second order accurate. The trade-off is the increased complexity of the implementation. We refer the readers to [45] for the details.

8. THE IMMERSED INTERFACE METHOD FOR PARABOLIC INTERFACE PROBLEMS

The IIM method has been developed for parabolic interface problems with fixed or moving interfaces.

8.1. The ADI method for the heat equation with a fixed interface

In [46], an alternating directional implicit (ADI) method was developed for the heat equations with singular source along a fixed interface Γ :

$$(8.1) \quad u_t = (u_x)_x + (u_y)_y - \int_{\Gamma} v(s, t) \delta(x - X(s)) \delta(y - Y(s)) ds.$$

The solution is allowed to have a jump $[u] = w$, as well. The interface relations

for the problem are:

$$(8.2) \quad \begin{aligned} [u] &= w, & [u_\eta] &= [u]_\eta = w_\eta(\eta, t), \\ [u_\xi] &= [u_n] = v(\eta, t), & [u_{\xi\xi}] &= \chi''[u_\xi] - w_{\eta\eta} + [f] + w_t, \\ [u_{\eta\eta}] &= -\chi''[u_\xi] + w_{\eta\eta}, & [u_{\xi\eta}] &= \chi''[u_\eta] + v_\eta. \end{aligned}$$

These jump relations can be easily decomposed into the x - and y -directions:

$$(8.3) \quad \begin{aligned} [u_x] &= [u_\xi] \cos \theta - [u_\eta] \sin \theta, & [u_y] &= [u_\xi] \sin \theta + [u_\eta] \cos \theta, \\ [u_{xx}] &= [u_{\xi\xi}] \cos^2 \theta - 2[u_{\xi\eta}] \cos \theta \sin \theta + [u_{\eta\eta}] \sin^2 \theta, \\ [u_{yy}] &= [u_{\xi\xi}] \sin^2 \theta + 2[u_{\xi\eta}] \cos \theta \sin \theta + [u_{\eta\eta}] \cos^2 \theta, \end{aligned}$$

where the θ is the angle between the normal direction and the x -axis. The finite difference equation is carefully constructed by incorporating the jump conditions in each direction as well as the cross derivative in the splitting:

$$(8.4) \quad \begin{aligned} \frac{u_{ij}^{n+\frac{1}{2}} - u_{ij}^n}{\Delta t/2} &= \delta_x u_{ij}^{n+\frac{1}{2}} - (C_x)_{ij}^{n+\frac{1}{2}} - Q_{ij}^n - R_{ij}^n + \delta_y u_{ij}^n - (C_y)_{ij}^n - f_{ij}^{n+\frac{1}{2}}, \\ \frac{u_{ij}^{n+1} - u_{ij}^{n+\frac{1}{2}}}{\Delta t/2} &= \delta_x u_{ij}^{n+\frac{1}{2}} - (C_x)_{ij}^{n+\frac{1}{2}} - Q_{ij}^n - R_{ij}^n + \delta_y u_{ij}^{n+1} - (C_y)_{ij}^{n+1} - f_{ij}^{n+\frac{1}{2}}, \end{aligned}$$

where Δt is the time step size and

$$\delta_x u_{ij}^n = (u_{i-1,j}^n - 2u_{ij}^n + u_{i+1,j}^n) / h^2, \quad \delta_y u_{ij}^n = (u_{i,j-1}^n - 2u_{ij}^n + u_{i,j+1}^n) / h^2.$$

At regular grid points, the standard ADI method is used, in which

$$(C_x)_{ij}^{n+\frac{1}{2}} = Q_{ij}^n = R_{ij}^n = (C_y)_{ij}^n = Q_{ij}^n = (C_y)_{ij}^{n+1} = 0.$$

At an irregular grid point, these correction terms are:

$$(8.5) \quad \begin{aligned} (C_x)_{ij} &= \frac{[u]}{h^2} + [u_x] \frac{(x_{i+1} - x^*)}{h^2} + [u_{xx}] \frac{(x_{i+1} - x^*)^2}{2h^2}, \\ Q_{ij}^n &= \frac{1}{2} \left((C_x)_{ij}^n + (C_x)_{ij}^{n+1} \right) - (C_x)_{ij}^{n+\frac{1}{2}}, \\ R_{ij}^n &= \pm \frac{[u_{yy}]^{n+1} - [u_{yy}]^n}{4 \Delta t}, \end{aligned}$$

where x^* is the intersection of the interface and the grid line $y = y_j$. The term $(C_y)_{ij}$ is similar to $(C_x)_{ij}$. The sign in the last expression above is determined

by the relative position of (x_i, y_j) and Γ . The method is accurate in the sense that it has global h^2 accuracy. It is efficient in the sense that it only needs to solve a sequence of tridiagonal system of equations at each time level.

The generalization of the ADI method for piecewise constant coefficient can be found in [74].

8.2. The maximum principle preserving scheme and a new multi-grid method for diffusion and convection equations with an interface

The ADI method is difficult to extend to interface problems with discontinuous and variable coefficients because the flux jump condition usually can not be easily decomposed in the x - and y - directions. In [2], Adams and Li have developed the maximum principle preserving scheme for the following two dimensional problems

$$(8.6) \quad \begin{aligned} u_t + \mathbf{a}(\mathbf{x}, t) \cdot \nabla u &= \nabla \cdot (\beta \nabla u) + f, & \mathbf{x} \in \Omega = \Omega^+ \cup \Omega^-, & \quad x \notin \Gamma, \\ [u]|_{\Gamma} = w(s), & & [\beta \mathbf{u}_n]|_{\Gamma} = v(s), \\ u(\mathbf{x}, 0) = u_0(\mathbf{x}), & & u(\mathbf{x}, t)|_{\partial\Omega} = g(\mathbf{x}, t). \end{aligned}$$

The diffusion term is discretized implicitly so that we can take large time steps, while the advection term is discretized explicitly so that second order accuracy can be achieved without affecting the discretization of the diffusion part. The discretization has the following form

$$(8.7) \quad \frac{u^{n+1} - u^n}{\Delta t} + (\mathbf{a} \cdot \nabla_h u)^{n+\frac{1}{2}} = \frac{1}{2} ((\nabla_h \cdot \beta \nabla_h u)^n + (\nabla_h \cdot \beta \nabla_h u)^{n+1}) + f^{n+\frac{1}{2}},$$

where

$$(8.8) \quad (\mathbf{a} \cdot \nabla_h u)^{n+\frac{1}{2}} = \frac{3}{2} (\mathbf{a} \cdot \nabla_h u)^n - \frac{1}{2} (\mathbf{a} \cdot \nabla_h u)^{n-1},$$

∇_h is the discrete gradient, and $t^{n+\frac{1}{2}} = t^n + \Delta t/2$. This discretization is second order accurate both in time and space. The CFL time step restriction is

$$\Delta t \leq \frac{h}{\sqrt{2} \|\mathbf{a}\|_2}.$$

The spatial discretization at irregular grid points is done through the maximum principle preserving IIM scheme discussed in Sec. 3. The implicit linear system of equations for u^{n+1} is solved using the new multigrid method designed for interface problems. We refer the readers to [2] for more details.

8.3. The IIM for 1D moving interface problems

In [41], the IIM was developed for the following non-linear moving interface problem

$$(8.9) \quad \begin{aligned} u_t + \lambda u u_x &= (\beta u_x)_x - f(x, t), \quad x \in [0, \alpha] \cup (\alpha, 1], \\ \frac{d\alpha}{dt} &= w(t, \alpha; u^-, u^+, u_x^-, u_x^+), \quad t > 0, \end{aligned}$$

with three different interface conditions listed below.

- The solution $u(\alpha, t) = r(t)$ is given at the interface. This is the case of 1D solidification problems.
- The jump conditions $[u] = q(t)$ and $[\beta u_x] = v(t)$ are given at the interface.
- The interface conditions $u(\alpha, t) = u_0$ and $\frac{d\alpha}{dt} = \sigma(t)[\beta u_x]$ are given. This kind of problems is called the Stefan problems.

The discretization is the Crank-Nicholson scheme for the governing equation and the trapezoidal rule for the motion

$$(8.10) \quad \begin{aligned} \frac{u_i^{n+1} - u_i^n}{\Delta t} - Q_i^{n+\frac{1}{2}} + \frac{\lambda}{2} (u_i^n u_{x,i}^n + u_i^{n+1} u_{x,i}^{n+1}) \\ = \frac{1}{2} \left((\beta u_x)_{x,i}^n + (\beta u_x)_{x,i}^{n+1} \right) - \frac{1}{2} (f_i^n + f_i^{n+1}), \\ \frac{\alpha^{n+1} - \alpha^n}{\Delta t} = \frac{1}{2} (w^n + w^{n+1}). \end{aligned}$$

The spatial discretization for u_x and $(\beta u_x)_x$ is done through the IIM discussed in the previous sections, see also [41] for the details, the correction term $Q_i^{n+\frac{1}{2}}$ is added when the interface $\alpha(t)$ crosses the grid line $x = x_i$ meaning that (x_i, t^n) and (x_i, t^{n+1}) are on the different sides of the interface. The correction term is determined from

$$(8.11) \quad Q_j^{n+\frac{1}{2}} = \frac{[u]_{;\tau}}{\Delta t} + \frac{1}{\Delta t} \left(t^{n+\frac{1}{2}} - \tau \right) [u_t]_{;\tau},$$

where the crossing time τ is estimated from the following equation

$$(8.12) \quad \frac{x_j - \alpha^n}{\tau - t^n} - \frac{\alpha^{n+1} - x_j}{t^{n+1} - \tau} = \frac{1}{2} (w^n - w^{n+1}).$$

The IIM has also been developed by Kandilarov for the following non-linear problems

$$(8.13) \quad u_t - (\beta u_x)_x + c(t)\delta(x - \xi(t))f(u) = F(x, t),$$

where $\xi(t)$ is a moving boundary, see [28].

9. APPLICATIONS OF THE IMMERSSED INTERFACE METHOD FOR MOVING INTERFACE/FREE BOUNDARY PROBLEMS

For moving interface/free boundary problems, it is not enough just to solve the differential equations with discontinuous coefficients and/or singular sources. We also need to locate moving interfaces to certain accuracy. There are three types of evolution schemes. The first one is the Lagrangian formulation that uses a set of ordered marked particles \mathbf{X}_k , $k = 1, 2, \dots$. The position of these marked points are updated according to some physical laws, typically $\frac{d\mathbf{X}}{dt} = \mathbf{u}$, where \mathbf{u} is the velocity. This method is also called the front tracking method and has many applications. But it may suffer from topological changes, e.g., when two “bubbles” merge or a single “bubble” splits, ad-hoc techniques are required. The entire system may become stiff when the particles become clustered together. On the other hand, the accuracy of the moving interface is easier to control since the interface is independent of the underlying grid. Also particle method has less grid orientation effects and can preserve the area better for the incompressible flow.

Another class of algorithms are the “volume of fluid” techniques, which track the motion of the interior region [6, 67]. These methods are more adaptable to topological changes but may lack the ability to compute geometrical quantities such as the curvature of the front, accurately.

The third method is the level set method originally proposed in [61]. If the interface at time t is the zero level set $\varphi(\mathbf{x}, t) = 0$, where $\varphi(\mathbf{x}, t)$ is defined on the entire domain, then we differentiate $\varphi(\mathbf{x}, t) = 0$ with respect to time t to get

$$(9.1) \quad \begin{aligned} & \varphi_t + \nabla\varphi \cdot \frac{d\mathbf{x}}{dt} = 0, \\ \text{or} \quad & \varphi_t + \left(\frac{\nabla\varphi}{|\nabla\varphi|} \cdot \mathbf{u} \right) |\nabla\varphi| = 0, \\ \text{or} \quad & \varphi_t + V|\nabla\varphi| = 0, \end{aligned}$$

where V is the normal velocity. The equation above is referred to as a Hamilton-Jacobi equation which can be solved efficiently using numerical methods for the conservation laws.

There are many advantages of the level set method. It is robust and simple to implement in any dimensions. It can easily handle topological changes. It often regularize a problem as well. The increased computational cost due to the embedding the interface into a higher dimensional space is relieved by the local level set method. It has been well known that a re-initialization process is crucial to the success of the level set method. We refer the reader to [60, 73] for more recent development in the level set method.

9.1. The IIM for the Stokes flow and the Navier-Stokes equations with a moving interface

The Stokes equations model the creeping flow of a highly viscous fluid, in the limit where the Reynolds number goes to zero and both the inertial acceleration and convection terms are dropped from the Navier-Stokes equations. The governing equations take the form

$$(9.2) \quad \begin{aligned} \nabla p &= \nabla \cdot \mu \nabla \mathbf{u} + \mathbf{F}, \\ \nabla \cdot \mathbf{u} &= 0, \quad \frac{d\mathbf{X}}{dt} = \mathbf{u}, \end{aligned}$$

where \mathbf{X} gives the location of the interface at time t . The time dependence of this problem is the driven force $\mathbf{F}(\mathbf{x}, t)$.

For an elastic boundary, following Peskin's immersed boundary method [79], the singular force can be written as

$$(9.3) \quad \mathbf{F}(\mathbf{x}, t) = \int_{\Gamma} \mathbf{f}(s, t) \delta(\mathbf{x} - \mathbf{X}(s, t)) ds,$$

and the force density \mathbf{f} is given by the Hooke's law

$$(9.4) \quad \mathbf{f} = \frac{\partial}{\partial s} (T(s) \boldsymbol{\tau}),$$

where $\boldsymbol{\tau} = \frac{\partial \mathbf{X}}{\partial s} / |\frac{\partial \mathbf{X}}{\partial s}|$, and $T(s) = T_0(|\frac{\partial \mathbf{X}}{\partial s}| - 1)$ is the tension of the immersed boundary. We assume periodic boundary conditions for \mathbf{u} and the pressure. The problem is well-posed³ except that the pressure can differ by a constant. We assume that μ is a constant.

As explained in [64, 79], the problem is very stiff. Explicit methods will suffer because of very small time step constraint due to the non-linearity associated with (9.2)-(9.4). Implicit or semi-implicit methods have been developed for this problem, see [64] for an overview.

This problem seems to be an ideal application of the IIM. Applying the gradient operator to the first equation in the interior domain excluding the interface Γ , and from the incompressibility condition, we get a Laplacian equation for the pressure. The Laplacian equation can be solved easily using the IIM. The cost is about one call to a fast Poisson solver. In this case, the pressure itself, and its normal derivative, are both discontinuous. Once the pressure is computed, the velocity can be computed by solving the two Poisson

³If a Dirichlet boundary condition is prescribed for the velocity, then there should be no boundary condition for the pressure.

equations for the velocity. For the isothermal flow, the velocity is continuous. But the other jump conditions are not explicitly given. In [39], using the distribution theory and the Green's theorem, the following jump conditions

$$(9.5) \quad \begin{aligned} [p](s) &= \hat{f}_1(s, t), & [p_n](s) &= \frac{\partial}{\partial s} \hat{f}_2(s, t), \\ [\mathbf{u}] &= 0, & [\mathbf{u}_n](s) &= \hat{f}_2(s, t) \boldsymbol{\tau}, \end{aligned}$$

(a) (b)

FIG. 9.1. (a) A stretched elastic membrane is relaxing to its equilibrium, a circle with $r = 0.3$. (b) A bubble rising. Both simulations are done using a 160×160 grid. The break-up of the bubble was captured easily with the level set method.

have been derived, where \hat{f}_1 and \hat{f}_2 are the projections of the force strength in the normal and the tangential directions respectively. With the jump conditions, the IIM can be used to solve the three Poisson equations at each time step to get the pressure and the velocity.

In Figure 9.1(a), we show a numerical simulation of the relaxation process of a stretched elastic membrane, the dotted line is the resting equilibrium membrane. Note that even in the equilibrium state, there is still a jump in the pressure which is balanced by the surface tension due to the stretch. In the simulation, we use a quasi-Newton method based on the BFGS (Broyden-Fletcher-Goldfarb-Shanno) rank-2 update to approximate the Jacobian matrix for the new location \mathbf{X} to treat the stiff system. The combination of the IIM and the quasi-Newton method worked very well [37]. Each step only took about $5 \sim 6$ iterations.

If the gravitational force is involved, and the force strength along the interface is $\mathbf{f}(t) = \tau_0 \kappa \mathbf{n}$, where κ is the curvature, the Stokes equation can be used to simulate a bubble motion within another fluid, see [37, 48]. However, the particle approach is not adequate to treat topological changes and the level set method is used in the simulation, see Figure 9.1(b).

The immersed interface method has also been developed [31] for the full

Navier-Stokes equations involving interface:

$$(9.6) \quad \begin{aligned} \rho \left(\frac{\partial \mathbf{u}}{\partial t} + (\mathbf{u} \cdot \nabla) \mathbf{u} \right) + \nabla p &= \mu \Delta \mathbf{u} + \mathbf{G} + \mathbf{F}, \quad \mathbf{x} \in \Omega, \\ \nabla \cdot \mathbf{u} &= 0, \\ \mathbf{u}|_{\partial\Omega} &= \mathbf{u}_b, \quad \text{BC}, \quad \mathbf{u}(\mathbf{x}, 0) = \mathbf{u}_0, \quad \text{IC}, \end{aligned}$$

where G is bounded and may have a finite jump across the interface. Here we write \mathbf{F} and \mathbf{G} separately to distinguish different irregularities. The singular force \mathbf{F} is the same as in (9.3). When μ is a constant, then the jump conditions (9.5) are still true in addition to the following:

$$(9.7) \quad \begin{aligned} [\mathbf{u}_\eta] &= \mathbf{0}, \quad [\mu \mathbf{u}_{\eta\eta}] = \kappa \hat{f}_2 \boldsymbol{\tau}, \quad [\mu \mathbf{u}_{\xi\eta}] = -\frac{\partial \hat{f}_2}{\partial \eta} \boldsymbol{\tau} - \kappa \hat{f}_2 \mathbf{n}, \\ [\mu \mathbf{u}_{\xi\xi}] &= -[\mu \mathbf{u}_{\eta\eta}] + [p_\xi] \mathbf{n} + [p_\eta] \boldsymbol{\tau} + [\mathbf{u}_\xi] \mathbf{u} \cdot \mathbf{n} - [\mathbf{G}], \end{aligned}$$

see [31, 32] for the derivation. The projection method for the Navier-Stokes equations is described below:

$$(9.8) \quad \begin{aligned} \frac{\mathbf{u}^* - \mathbf{u}^n}{\Delta t} + (\mathbf{u} \cdot \nabla_h \mathbf{u})^{n+\frac{1}{2}} &= \nabla_h p^{n-\frac{1}{2}} + \frac{\mu}{2} (\Delta_h \mathbf{u}^* + \Delta_h \mathbf{u}^n) + \mathbf{G}^{n+\frac{1}{2}} + \mathbf{C}_1^n, \\ \mathbf{u}^*|_{\partial\Omega} &= \mathbf{u}_b^{n+1}, \end{aligned}$$

where $(\mathbf{u} \cdot \nabla_h \mathbf{u})^{n+\frac{1}{2}}$ is approximated by

$$(9.9) \quad (\mathbf{u} \cdot \nabla_h \mathbf{u})^{n+\frac{1}{2}} = \frac{3}{2} (\mathbf{u}^n \cdot \nabla_h) \mathbf{u}^n - \frac{1}{2} (\mathbf{u}^{n-1} \cdot \nabla_h) \mathbf{u}^{n-1} + \mathbf{C}_2^n.$$

The projection step is the following:

$$(9.10) \quad \begin{aligned} \Delta_h \phi^{n+1} &= \frac{\nabla_h \cdot \mathbf{u}^*}{\Delta t} + \mathbf{C}_3^n, \quad \left. \frac{\partial \phi^{n+1}}{\partial \mathbf{n}} \right|_{\partial\Omega} = 0, \\ \mathbf{u}^{n+1} &= \mathbf{u}^* - \Delta t \nabla_h \phi^{n+1} + \mathbf{C}_4^n, \\ \nabla_h p^{n+1/2} &= \nabla_h p^{n-1/2} + \nabla_h \phi^{n+1} + \mathbf{C}_5^n. \end{aligned}$$

All the correction terms C_l^n are determined from the IIM using the jump relations which can be decomposed in the x - and y - directions.

The IIM method for the Navier-Stokes equations have been well tested both against the exact solutions and common flow problems. In Fig. 9.2, we show an example of a fixed interface. The driven force of the flow is a fixed tangential force. Therefore the steady state solution of the flow is a steady rotation along the circular interface. In Fig. 9.2 (a), we plot the x - component

of the velocity $-u(x, y)$ at $t = 10$ computed using a 64 by 64 grid. We can see clearly the non-constant jump in the normal derivative. In Fig. 9.2 (b), we plot the velocity field at $t = 10$ which shows the rotation due to the uniform tangential force.

9.2. Simulations of the Hele-Shaw flow and crystal growth

In the oil industry, water (less viscous fluid) sometimes is injected to oil (more viscous fluid) wells to increase the pressure for higher yield of oil. The interaction

(a) (b)

FIG. The computed steady state velocity with a 64×64 grid, see Example 4 in 9.2. [31]. The interface is a fixed circle $r = 0.5$. Other parameters are $\mathbf{G} = \mathbf{0}$, $\hat{f}_1 = 0$, $\hat{f}_2 = 10$, and $\mu = 0.02$. The time step size is $\Delta t = h$. (a) Plot of $-u(x, y)$ at $t = 10$ which is not smooth. (b) The plot of the velocity field at $t = 10$, the flow approaches a steady rotation along the interface.

between the less viscous and more viscous fluids can be modeled as a Hele-Shaw flow, see [70]. In the Hele-Shaw flow, the shape of the interface is well known to exhibit a fingering phenomenon. The velocity field \mathbf{u} of the flow is proportional to the gradient of the pressure p

$$(9.11) \quad \mathbf{u} = -\beta \nabla p, \quad \nabla \cdot \mathbf{u} = \phi,$$

where β is a piecewise constant associated with the viscosity μ , which is very different inside and outside the interface separating the two fluids. The source term ϕ is the result of the injection of the less viscous fluid into the Hele-Shaw cell. Usually ϕ has a compact support. The jump conditions across the interface are

$$(9.12) \quad \begin{aligned} [p] &= \tau \kappa, & \text{the Laplace-Young Condition,} \\ [\beta p_n] &= 0, & \text{the kinematic interface condition,} \end{aligned}$$

where τ is the surface tension and κ is the curvature of the interface.

From the linearization analysis, we have obtained a Mullins-Sekerka type instability in [19], which shows the competition between the de-stabilizing effect due to the injection and the stabilizing effect due to the surface tension. The analysis revealed very interesting discovery that the very high or very low frequency modes are actually stable, but some middle frequency modes can be unstable. Usually it is relatively easier to control high frequency noises.

But it is more difficult to control the round-off errors of low to intermediate frequency modes.

FIG. 9.3. The numerical simulation of an expanding Hele-Shaw bubble with initial interface: $\rho = 0.2 + 0.05 \sin(3\theta)$, $0 \leq \theta \leq 2\pi$, the surface tension is 1.257×10^{-3} . The grid size is 320 by 320.

This problem can be easily solved using the IIM since (9.11) can be written as

$$(9.13) \quad \nabla \cdot (\beta \nabla p) = -\phi,$$

and we know the jump conditions (9.12). We can apply the fast IIM discussed in Sec. 4 to solve the pressure, then use an interpolation scheme to compute the gradient of the pressure to get the velocity. After applying the fast IIM again to get the velocity, the interface is evolved by the fast level set method. We show one example of an expanding Hele-shaw bubble in Fig. 9.3 which is similar to the one computed in [20]. While the boundary integral method can be more accurate if there are enough control points, the IIM combined with the level set method gives reasonable good result in much shorter time. More important, topological changes can be handled easily. Other examples and more details can be found in [19].

The Stefan problems for solidification process and unstable crystal growth are among many important free boundary/moving interface problems. In [33], Langer has given an easily understood, but insightful description of the problem which we briefly explain below. Consider two typical cases involving the same substance but at different states, liquid and solid states, as shown in Fig. 9.4. In both cases, a pure fluid is contained in a vessel whose walls are held at some temperature T_W which is less than the melting temperature T_M . In the first case, the liquid is initially at a temperature $T \geq T_M$, and the solid is allowed to start forming at the walls. In this case, the process is completely stable. The solidification front Γ moves smoothly and uniformly toward the

center. Such a process is often referred to as a stable Stefan problem. The second case, Fig. 9.4 (b), is more interesting. Now the liquid is initially under-cooled to a temperature $T < T_M$, and the solidification is initiated

(a) (b)

FIG. Schematic illustration of solidification occurring in a stable configuration 9.4. (a); in an unstable configuration (b), see [33].

at a seed crystal at the center. The situation is intrinsically unstable. The moving front Γ develops unstable dendrites. Such processes have wide applications in the aerospace, semi-conductor, and medical industries.

There are primarily two kinds of mathematical models for Stefan problems and crystal growth. One is the phase field model that introduces an additional field variable to track the phase, and the interface is represented by a region of nonzero thickness, see Kobayashi [30], Braun [8], and the references therein. Another type of models is the sharp interface models in which the interface between two phases is represented by a curve in two space dimensions, and a surface in three dimensions. Each model has its merits and limitations and corresponds to certain applications. A variety of methods have been reported in the literature. We refer the reader to [27] for a complete review of the different methods.

A simple but widely accepted sharp interface model consists of the heat equation for the temperature

$$(9.14) \quad \rho c \frac{\partial T}{\partial t} = \nabla \cdot (\beta \nabla T),$$

where ρ is the density, c is the heat capacity, and β is the thermal conductivity, respectively, see [13]. Generally these quantities are discontinuous across the moving front. The normal velocity of the moving front is coupled by the change in the heat flux

$$(9.15) \quad \rho L V = - \left[\beta \frac{\partial T}{\partial \mathbf{n}} \right],$$

where L is the latent heat of solidification. For the classical Stefan problems,

the temperature at the front is a constant

$$(9.16) \quad T(\mathbf{x}, t) = T_M,$$

which is the melting temperature. For problems involving crystal growth, we should consider the Gibbs-Thomson relation

$$(9.17) \quad T(\mathbf{x}, t) = -\epsilon_C \kappa - \epsilon_V V,$$

where κ is the curvature, ϵ_C is the surface tension coefficient, and ϵ_V is the molecular kinetic coefficient. In the isotropic case, both ϵ_C and ϵ_V are constants. For the anisotropic case, they have the following form

$$(9.18) \quad \begin{aligned} \epsilon_C &= \bar{\epsilon}_C(1 - A \cos(\beta_A \theta + \theta_o)), \\ \epsilon_V &= \bar{\epsilon}_V(1 - A \cos(\beta_A \theta + \theta_o)), \end{aligned}$$

where θ is the angle between the x -axis and n , and θ_o controls the angle of the symmetry axis upon which the crystal grows. The constant A , β_A , θ_o , $\bar{\epsilon}_C$ and $\bar{\epsilon}_V$ depend on materials involved.

In [49], we have developed a second order alternating directional implicit (ADI) method coupled with the level set method for the Stefan problems and crystal growth. We use the standard ADI scheme away from the interface, and the backward Euler scheme at irregular grid points near or on the interface. The global error in the maximum norm still has second order convergence. It is necessary to add a correction term when the interface crosses the grid lines between different time levels. Theoretically we have shown that the ADI method is asymptotically stable. The weighted least squares interpolation (WLSI) scheme is used to restrict the information of a grid function to the interface. The information on the interface, for example, the normal velocity which is only defined on the interface, is extended to the grid points.

In Fig. 9.5, we show several simulations of crystal growth with difference surface tension and latent heat. The simulation results agree with those results in the literature and experiments. The method has also been checked against the exact solutions.

9.3. The surface Laplacian and the simulation of electro-migration of voids

In many physical problems, mass transport along interfaces such as surface diffusion and grain boundary diffusion becomes increasingly important as the characteristic length scale is reduced. The diffusional mass transport is governed by a relevant chemical potential along the interface. The dynamics of these processes is of great interest to material scientists and biologists. There

is a large literature on this topic. We refer the readers to two recent survey articles by Mullins [58], and Cahn and Taylor [9] and the references therein. In [51], a mathematical model has been developed for the surface diffusion involving the evolution of voids under electro-migration in a conducting metal line. The normal velocity of the void surface is given by

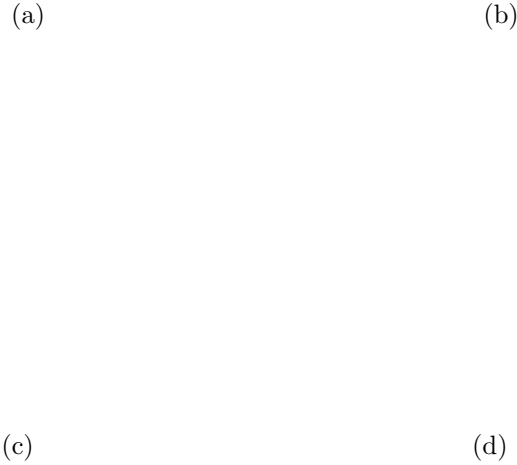


FIG. 9.5. Crystal growth with different surface tension and latent heat. The heat conductivity is $\beta^+ = \beta^- = 1$. The initial boundary of the seed in the polar coordinates is $r = 0.5 + 0.03 \cos(l\theta)$, $0 \leq \theta \leq 2\pi$ with $l = 4$ for (a)-(c), and $l = 5$ for (d). All the simulations are computed using a 320 by 320 grid. The latent heat is $L = 1/0.8 = 1.25$ for (b)-(d) except for (a) which is $L = 1/0.5$. (a) $\epsilon_C = 0.0051$, $\epsilon_v = 10^{-5}$; (b) $\epsilon_c = 0.01$, $\epsilon_v = 0$, (c) $\epsilon_C = 0.001$, $\epsilon_v = 0.001$; (d) $\epsilon_C = 10^{-4}$, $\epsilon_v = 0$. As the surface tension ϵ_C decreases, we see that more dendrites are formed.

$$(9.19) \quad U_n = \Delta_s(C_1\phi + C_2\kappa),$$

where Δ_s is the surface Laplacian, ϕ is the potential associated with an applied electric field, and κ is the mean curvature along the boundary corresponding to the chemical potential. The potential function ϕ satisfies a Poisson equation in the exterior of the voids with a homogeneous Neumann boundary condition along the boundary of the voids. The time evolution equation for the curvature κ with respect to the arc length s is

(a) (b)

FIG. 9.6. A void evolution with different electric and chemical potentials. (a) The chemical potential constant, $C_2 = 3.9062 \times 10^{-4}$, is small compared to that of electrical potential constant, $C_1 = 1.875$, and the motion is less stable. (b) The coefficients are $C_1 = 1.875$ and $C_2 = 0.3.90625 \times 10^{-3}$. The motion is relatively stable because C_2 is larger than that in (a).

$$(9.20) \quad \kappa_t = -\kappa^2 \kappa_{ss} - \kappa_{ssss}.$$

In [51], the fast Poisson solver for irregular domains discussed in Sec. 4.1 was used to solve the electric potential outside the voids. The surface Laplacian of a two dimensional function f is computed as

$$\Delta_s f = \frac{d^2 f}{ds^2} = \frac{d}{ds}(\boldsymbol{\tau} \cdot \nabla f) = \kappa \mathbf{n} \cdot \nabla f + \boldsymbol{\tau}^T He(f) \boldsymbol{\tau} = \kappa \frac{\partial f}{\partial n} + \Delta f - \frac{\partial^2 f}{\partial n^2}.$$

In Fig. 9.6 we show two simulations of electro-migration of voids. The first one is a single void with small chemical potential compared to the electrical potential. Our simulation has gone beyond the results obtained in [82]. The evolution process seems to agree with the results in that paper up to some time. In the second simulation, we investigate the effect of initial shape of a void. While the surface tension force tends to smooth the void shape into a circle, the electrical potential causes a protrusion of the void with a relatively large curvature at the frontal tip of the void. This sharp tip moves rapidly under the electro-migration forces and drags the rest of the void along. Such a worm-like motion of void demonstrates another delicate balance between surface tension and electro-migration forces. More examples and analysis can be found in [51].

9.4. Other applications of the IIM

We list below other applications of the IIM without too much elaborations. In [47], the IIM is used to calculate the temperature profile of a growing continental ice sheet. In that problem, there is one fixed interface between the ice sheet and the rock, and a free boundary which is the height of the ice sheet. In [52], the IIM method was used to solve a thermoelastic system which models a homogeneous and isotropic bar made of two distinct materials. The system contains a parabolic equation and is coupled with a hyperbolic equation. A new transformation was proposed to analyze and solve the problem numerically.

Another important application of the IIM is an inverse problem in electrical impedance tomography. We have developed a mathematical model and a numerical method to identify unknown objects within a body from the measured data in narrow strip of the boundary [44]. The fast Poisson solver for irregular domains once again is used. The problem is equivalent to identify the coefficient of the conductivity in the potential equation and is modeled as a variational form which is ill-posed. The use of the level set function actually is a regularization factor. The three dimensional simulations can be found in [15, 16].

Recently, the IIM has been developed for non-linear elliptic interface problems of the form

$$(9.21) \quad -\nabla \cdot (\beta(\mathbf{x}, |\nabla u|) \nabla u) = f,$$

where $\beta(\mathbf{x}, |\nabla u|)$ may be discontinuous across interfaces in the solution domain, see [23]. The non-linearity is the dependency of the coefficient β on the gradient of the solution. This kind of non-linear PDEs have many applications, for example, the magneto-rheological (MR) fluids that contain iron particles [54], and the minimal surface problems etc. To solve the equation (9.21), a substitution method

$$(9.22) \quad -\nabla \cdot (\beta(\mathbf{x}, |\nabla u^k|) \nabla u^{k+1}) = f,$$

$$(9.23) \quad [u^{k+1}] = w^k(s), \quad \left[\beta(\mathbf{x}, |\nabla u^k|) u_n^{k+1} \right] = v^k(s),$$

for u^{k+1} is used, where $w^k(s)$ and $v^k(s)$ are determined from the physical problems. The convergence of the substitution method for certain non-linear problems is proved in [23]. The linearized problem is solved using the maximum principle preserving IIM method.

In Fig. 9.7, we show some numerical solution to the non-linear equation used to model the MR-fluid containing metal particles. We want to find out

how the metal particles line-up under different electric field. Boundary integral methods can not be applied because there is no green function for the non-linear problem. Finite element methods with body fitted grid are very expensive because the mesh generation and the computation of the non-linear coefficient. Our substitution method coupled with

(a) (b)

FIG. 9.7. The contour plots of potential function of magneto-rheological (MR) fluid containing metal particles obtained from the substitution method. (a) Single particle with different applied electric fields. The figure at the bottom has stronger field. Dirichlet boundary condition is used. The mesh size is 256×128 . (b) Multi-particles with different applied electric fields. The plot to the right has stronger field. A periodic boundary condition is used. The mesh size is 320×640 .

the maximum principle preserving scheme as the linear solver is efficient and accurate. In Fig. 9.7 (a), we show the equi-potential of a single particle with different applied field. Our results agree with those in the literature [54]. In Fig. 9.7 (b), we show the results under different electric applied fields with multi-particles and more realistic but more difficult boundary conditions.

10. OTHER NUMERICAL METHODS RELATED TO THE IMMERSSED INTERFACE METHOD

The IIM has been well recognized because of its merits. Several new methods based on the IIM have been developed. In this section, we give an incomplete review of those related methods.

10.1. The IIM for hyperbolic equations

LeVeque and Zhang extended the IIM for hyperbolic equations including one and two dimensional acoustic wave equations, two dimensional elasticity equations [38, 84]. Interface relations have been derived for those systems and used in constructing the finite difference schemes. Non-smooth interfaces

are allowed in their methods. Although the techniques that they used are based on finite difference discretizations, some of the techniques have been successfully merged with the finite volume implementation in the Clawpack [35]. Such combination is also used to solve the incompressible Navier-Stokes equations for two phase flow [34], and on irregular domains using the vorticity stream-function formulation [10, 11].

Recently, Piraux and Lombard [65] have proposed an explicit simplified interface method (ESIM) for hyperbolic interface problems. The finite difference equations at irregular grid points are constructed implicitly through an explicit modification of numerical values used for time-stepping. The modification is based on the spring-mass conditions satisfied at the interface.

Jovanović and Vulkov have studied parabolic and hyperbolic equations with unbounded coefficients of the following form

$$(10.1) \quad [c(x) + K \delta(x - \xi)] \frac{\partial^2 u}{\partial t^2} - \frac{\partial}{\partial x} \left(a(x) \frac{\partial u}{\partial x} \right) = f(x, t), \quad (x, t) \in (0, 1) \times (0, T),$$

where $0 < c_1 \leq a(x) \leq c_2$, $0 < c_3 \leq c(x) \leq c_4$, and c_i and $K > 0$ are constants. An abstract operator method is proposed for studying these equations. Estimates for the rate of convergence of the averaging operator difference schemes on special energetic Sobolev's norms, compatible with the smoothness of the solutions, are obtained, see [25, 26] and the reference therein.

10.2. The explicit jump immersed interface method (EJIIM)

Motivated by the fast IIM discussed in Sec. 4, Bube and Wiegmann developed the EJIIM for elliptic interface problems [80, 81]. The EJIIM works by focusing on the jumps in the solution and their derivatives, rather than on finding coefficients of a new finite difference scheme. As we mentioned earlier in this paper, if we know the jumps in $[u]$, $[u_x]$, $[u_y]$, $[u_{xx}]$, $[u_{yy}]$, etc., then we can use the standard finite difference method at all grid points plus some correction terms at irregular grid points. The EJIIM takes advantage of this property and expresses all the quantities in term of the original jump conditions and the limiting values from a particular side, say, u^- , u_x^- , u_y^- , u_{xx}^- etc. These quantities are used as augmented unknowns. The bigger system of equations that involves the solution of the PDE at grid points and those limiting values at the interface is solved by the GMRES method. The EJIIM has been applied to two dimensional elastic equation in shape design in conjunction with the level set method [72].

10.3. The ghost fluid method (GFM)

The GFM was first used to properly treat the boundary conditions and remove the spurious oscillations for hyperbolic system. Liu, Fedkiw, and Kang

developed the GFM for elliptic interface problems in [53]. One of the motivations of the GFM is to simplify and symmetrize the IIM. The GFM is a sharp interface method because it builds in the jump conditions in the finite difference scheme. However, the GFM is generally first order accurate in the maximum norm if the coefficient is discontinuous. Essentially the GFM decomposes the flux jump in each axis direction so that the problem can be treated dimension by dimension. The main error of the GFM comes from the decomposition of the flux jump conditions because it is hard to do it accurately. The main advantage of the GFM is that it is simple, and is relatively easier to implement, and the system of finite difference equations is symmetric for self-adjoint elliptic problems. The GFM has been applied to multiphase incompressible flow [29], two phase incompressible flames simulations [59], and other applications.

11. OPEN PROBLEMS AND ACKNOWLEDGMENTS

The immersed interface method is an efficient sharp interface method for PDEs that involve discontinuities in the coefficients, the solution and its derivatives, and the Dirac delta function in the source term. The IIM is based on Cartesian grids with second order accuracy. It can be, and has been coupled with evolution schemes such as particle methods, the level set method, for free boundary and moving interface problems in two and three dimensions.

There are still some challenging problems for the IIM. (1) It is desirable to develop a second order conservative finite difference scheme for self-adjoint elliptic and parabolic interface problems based on Cartesian grids. (2) It is desirable to have the system of finite difference equations to be *symmetric* positive definite. (3) It is desirable to simplify the immersed interface method further and/or develop a reliable IIM software package. (4) It is desirable to have a simple and accurate (second order accurate) finite element method for interface problems. (5) It is not clear how to apply the IIM for problems in which the jump conditions are not explicitly given, or coupled together through some non-linear relations. (6) Theoretically, the convergence properties of the IIM need further investigation for moving interface/free boundary problems.

The author would like to thank the National Center for Theoretical Sciences (NCTS) of Taiwan for their support during his visit there (May 8, 2001–June 8, 2001).

REFERENCES

1. L. M. Adams, A multigrid algorithm for immersed interface problems, pages 1-14. Proceedings of Copper Mountain Multigrid Conference, NASA Conference Publication 3339, 1995.

2. L. M. Adams and Z. Li, The immersed interface/multigrid method for interface problems, *SIAM J. Sci. Comput.*, **24** (2002), 463-479.
3. J. B. Bell, C. N. Dawson, and G. R. Shubin, An unsplit, higher order Godunov method for scalar conservation laws in multiple dimensions, *J. Comput. Phys.*, **74** (1988), 1-24.
4. M. J. Berger and R. J. LeVeque, Adaptive mesh refinement using wave-propagation algorithms for hyperbolic systems, *SIAM J. Numer. Anal.*, **35** (1998), 2298-2316.
5. R. P. Beyer and R. J. LeVeque, Analysis of a one-dimensional model for the immersed boundary method, *SIAM J. Numer. Anal.*, **29** (1992), 332-364.
6. J. Brackbill, D. Kothe, and C. Zemach, A continuum method for modeling surface tension, *J. Comput. Phys.*, **100** (1992), 335-353.
7. J. Bramble and J. King, A finite element method for interface problems in domains with smooth boundaries and interfaces. *Advances in Comput. Math.*, **6** (1996), 109-138.
8. R. J. Braun, Adaptive phase-field computation of dendritic crystal growth, *J. Crystal Growth*, **174** (1997), 41-43.
9. J. W. Cahn and J. E. Taylor, Surface motion by surface diffusion, *Acta Metallica Materiala*, **42** (1994), 1045-1063.
10. D. Calhoun, *A cartesian grid method for solving the streamfunction-vorticity equations in irregular geometries*, PhD thesis, University of Washington, 1999.
11. D. Calhoun, A cartesian grid method for solving the streamfunction-vorticity equation in irregular regions, *J. Comput. Phys.*, **176** (2002), 231-275.
12. Z. Chen and J. Zou, Finite element methods and their convergence for elliptic and parabolic interface problems, *Numer. Math.*, **79** (1998), 175-202.
13. J. Crank, *Free and Moving Boundary Problems*, Oxford University Press, 1984.
14. D. De Zeeuw, Matrix-dependent prolongations and restrictions in a blackbox multigrid solver, *J. Comput. Appl. Math.* **33** (1990), 1-27.
15. S. Deng, Immersed interface method for three dimensional interface problems and applications, Ph.D thesis. North Carolina State University, 2000.
16. S. Deng, K. Ito, and Z. Li, Three dimensional elliptic solvers for interface problems and applications, *J. of Comput. Phys.*, in press, 2002.
17. M. Dumett and J. Keener, A numerical method for solving anisotropic elliptic boundary value problems on an irregular domain in 2D, *J. Comput. Phys.*, in press, 2002.
18. A. L. Fogelson and J. P. Keener, Immersed interface methods for Neumann and related problems in two and three dimensions, *SIAM J. Sci. Comput.*, **22** (2000), 1630-1684.

19. T. Hou, Z. Li, S. Osher, and H. Zhao, A hybrid method for moving interface problems with application to the Hele-Shaw flow, *J. Comput. Phys.*, **134** (1997), 236-252.
20. T. Y. Hou, J. S. Lowengrub, and M. J. Shelley, Removing the stiffness from interfacial flows with surface tension, *J. Comput. Phys.*, **114** (1994), 312-338.
21. H. Huang and Z. Li, Convergence analysis of the immersed interface method, *IMA J. Numer. Anal.*, **19** (1999), 583-608.
22. J. Hunter, Z. Li, and H. Zhao, Autophobic spreading of drops., *J. Comput. Phys.*, in press, also NCSU CRSC-TR99-31, 1999.
23. K. Ito and Z. Li, The immersed interface method for nonlinear interface problems with an application, submitted, 2002.
24. H. Johansen and P. Colella, A Cartesian grid embedded boundary method for Poisson equations on irregular domains. *J. Comput. Phys.*, **147** (1998), 60-85.
25. B. S. Jovanović and L. G. Vulkov, On the convergence of finite difference schemes for parabolic problems with concentrated data, *Numer. Math.*, **89** (2001), 715-734.
26. B. S. Jovanović and L. G. Vulkov, On the convergence of finite difference schemes for hyperbolic problems with concentrated data, *SIAM J. Numer. Anal.*, in press, 2002.
27. D. Juric and G. Tryggvason, A front-tracking method for dendritic solidification. *J. Comput. Phys.*, **123** (1996), 127-1487.
28. J. D. Kandilarov, Immersed interface method for a reaction-diffusion equation with a moving own concentrated source, Fifth Conf. on Numer. Meth. and Appls, August 20-24, 2002, Borovets, Bulgaria. (accepted in Lect. Notes in Math., Springer).
29. M. Kang, R. Fedkiw, and X. Liu, A boundary condition capturing method for multiphase incompressible flow, *J. Sci. Comput*, **15** (2000), 323-360.
30. R. Kobayashi, Modeling and numerical simulations of dendritic crystal-growth. *Physica D*, **63** (1993), 410-423.
31. M-C. Lai and Z. Li, The immersed interface method for the Navier-Stokes equations with singular forces, *J. Comput. Phys.*, **171** (2001), 822-842.
32. M-C. Lai and Z. Li, A remark on jump conditions for the three-dimensional Navier-Stokes equations involving an immersed moving membrane, *Applied Math. Letters*, **14** (2001), 149-154.
33. J. S. Langer, Instabilities and pattern formation in crystal growth, *Rev. of Modern Phys*, **52** (1980), 1-28.
34. L. Lee and R. J. LeVeque, An immersed interface method for incompressible Navier Stokes equations, preprint, 2002.

35. R. J. LeVeque, Clawpack and Amrclaw – Software for high-resolution Godunov methods. 4-th Intl. Conf. on Wave Propagation, Golden, Colorado, 1998.
36. R. J. LeVeque and Z. Li, The immersed interface method for elliptic equations with discontinuous coefficients and singular sources, *SIAM J. Numer. Anal.*, **31** (1994), 1019-1044.
37. R. J. LeVeque and Z. Li, Immersed interface method for Stokes flow with elastic boundaries or surface tension, *SIAM J. Sci. Comput.*, **18** (1997), 709-735.
38. R. J. LeVeque and C. Zhang, Immersed interface methods for wave equations with discontinuous coefficients. *Wave Motion*, **25** (1997), 237-263.
39. Z. Li, *The Immersed Interface Method — A Numerical Approach for Partial Differential Equations with Interfaces*, PhD thesis, University of Washington, 1994.
40. Z. Li, A note on immersed interface methods for three dimensional elliptic equations, *Computers Math. Appl.*, **31** (1996), 9-17.
41. Z. Li, Immersed interface method for moving interface problems, *Numerical Algorithms*, **14** (1997), 269-293.
42. Z. Li, A fast iterative algorithm for elliptic interface problems, *SIAM J. Numer. Anal.*, **35** (1998), 230-254.
43. Z. Li, The immersed interface method using a finite element formulation, *Applied Numer. Math.*, **27** (1998), 253-267.
44. Z. Li and K. Ito, Maximum principle preserving schemes for interface problems with discontinuous coefficients, *SIAM J. Sci. Comput.*, **23** (2001), 1225-1242.
45. Z. Li, T. Lin, and X. Wu, New Cartesian grid methods for interface problem using finite element formulation, *NCSU CRSC-TR99-5*, 1999.
46. Z. Li and A. Mayo, ADI methods for heat equations with discontinuities along an arbitrary interface, In *Proc. Symp. Appl. Math.* W. Gautschi, editor, volume 48, pages 311-315. AMS, 1993.
47. Z. Li, D. McTigue, and J. Heine, A numerical method for diffusive transport with moving boundaries and discontinuous material properties, *International J. Numer. & Anal. Method in Geomechanics*, **21** (1997), 653-662.
48. Z. Li and Y. Shen, Numerical method for simulation of bubbles flowing through another fluid, In Z.-C. Shi, W. M. Xue, M. Mu, and J. Zou, editors, *Advances in Scientific Computing*, pages 74-81. China Science Publisher, 2000.
49. Z. Li and B. Soni, Fast and accurate numerical approaches for Stefan problems and crystal growth, *Numerical Heat Transfer, B: Fundamentals*, **35** (1999), 461-484.
50. Z. Li, W-C. Wang, I-L. Chern, and M-C. Lai, New formulation and fast poisson solvers for interface problems in polar coordinates, *NCSU CRSC-TR01-24*, 2001.

51. Z. Li, H. Zhao, and H. Gao, A numerical study of electro-migration voiding by evolving level set functions on a fixed cartesian grid, *J. Comput. Phys.*, **152** (1999), 281-304.
52. Z. Li and J. Zou, Theoretical and numerical analysis on a thermo-elastic system with discontinuities, *J. of Comput. Appl. Math.*, **91** (1998), 1-22.
53. X. Liu, R. Fedkiw, and M. Kang, A boundary condition capturing method for Poisson's equation on irregular domain, *J. Comput. Phys.*, **160** (2000), 151-178.
54. H. Ly, M. Jolly, F. Reitich, K. Ito, and H. T. Banks, Piecewise linear models for field-responsive fluids, *IEEE Transaction on Magnetics*, **37** (2001), 558-560.
55. A. Mayo, The fast solution of Poisson's and the biharmonic equations on irregular regions, *SIAM J. Numer. Anal.*, **21** (1984), 285-299.
56. A. McKenney, L. Greengard, and Anita Mayo, A fast poisson solver for complex geometries, *J. Comput. Phys.*, (1995) 118.
57. K. W. Morton and D. F. Mayers, *Numerical Solution of Partial Differential Equations*, Cambridge press, 1995.
58. W. W. Mullins, Mass transport at interface in single component systems, *Metal. Trans. A*, **26** (1995), 1917-1929.
59. D. Nguyen, R. Fedkiw, and M. Kang, A boundary condition capturing method for incompressible flame discontinuities, UCLA CAM report #00-19, 2000.
60. S. Osher and R. Fedkiw, *Level Set Methods and Dynamic Implicit Surfaces*, Springer, New York, 2002.
61. S. Osher and J. A. Sethian, Fronts propagating with curvature-dependent speed: Algorithms based on Hamilton-Jacobi formulations, *J. Comput. Phys.*, **79** (1988), 12-49.
62. C. S. Peskin, Numerical analysis of blood flow in the heart, *J. Comput. Phys.*, **25** (1977), 220-252.
63. C. S. Peskin, Lectures on mathematical aspects of physiology, *Lectures in Appl. Math.*, **19** (1981), 69-107.
64. C. S. Peskin, The immersed boundary method, *Acta Numerica*, (2002), 1-39.
65. J. Piraux and B. Lombard, A new interface method for hyperbolic problems with discontinuous coefficients. One-dimensional acoustic example, *J. Comput. Phys.*, **168** (2001), 227-248.
66. W. Proskurowski and O. Widlund, On the numerical solution of Helmholtz's equation by the capacitance matrix method, *Math. Comp.*, **30** (1976), 433-468.
67. E. G. Puckett, A. S. Almgren, J. B. Bell, D. L. Marcus, and W. J. Rider, A high-order projection method for tracking fluid interfaces in variable density incompressible flows, *J. Comput. Phys.*, **130** (1997), 269-282.

68. J. W. Ruge and K. Stuben, Algebraic multigrid, In S. F. McCormick, editor, *Multigrid Method*, SIAM, Philadelphia, 1987.
69. Y. Saad, GMRES: A generalized minimal residual algorithm for solving non-symmetric linear systems, *SIAM J. Sci. Stat. Comput.*, **7** (1986), 856-869.
70. P. G. Saffman and G. I. Taylor, The penetration of a fluid into a porous medium or Hele-Shaw cell containing a more viscous liquid, *Proc. R. Soc. Lond. A*, **245** (1958), 312-329.
71. K. Schittkowski, QL-quadratic Programming, version 1.5, 1991.
<http://www.uni-bayreuth.de/departments/math/~kschittkowski/ql.htm>.
72. J. Sethian and A. Wiegmann, Structural boundary design via level set and immersed interface methods, *J. Comput. Phys.*, **163** (2000), 489-528.
73. J. A. Sethian, *Level Set Methods and Fast Marching methods*, Cambridge University Press, 2nd edition, 1999.
74. Y. Shen and Z. Li, A numerical method for solving heat equations involving interfaces, *Electron. J. Diff. Eqns.*, (2000), 100-108.
75. G. R. Shubin and J. B. Bell, An analysis of the grid orientation effect in numerical simulation of miscible displacement, *Comp. Meth. Appl. Mech. Eng.*, **47** (1984), 47-71.
76. M. Sussman, P. Smereka, and S. Osher, A level set approach for computing solutions to incompressible two-phase flow, *J. Comput. Phys.*, (1994), 114.
77. Paul N. Swarztrauber, Fast Poisson solver, In *Studies in Numerical Analysis*, G. H. Golub, editor, volume 24, pages 319-370. MAA, 1984.
78. A. N. Tikhonov and A. A. Samarskii, Homogeneous difference schemes, *USSR Comput. Math. and Math. Phys.*, **1** (1962), 5-67.
79. C. Tu and C. S. Peskin, Stability and instability in the computation of flows with moving immersed boundaries: a comparison of three methods, *SIAM J. Sci. Stat. Comput.*, **13** (1992), 1361-1376.
80. A. Wiegmann, *The explicit jump immersed interface method and interface problems for differential equations*, PhD thesis, University of Washington, 1998.
81. A. Wiegmann and K. Bube, The immersed interface method for nonlinear differential equations with discontinuous coefficients and singular sources, *SIAM J. Numer. Anal.*, **35** (1998), 177-200.
82. L. Xia, A. F. Bower, Z. Suo, and C. Shih, A finite element analysis of the motion and evolution of voids due to strain and electromigration induced surface diffusion, *J. Mech. Phys. Solids*, **45** (1997), 1473-1493.
83. Z. Yang, *A Cartesian grid method for elliptic boundary value problems in irregular regions*, PhD thesis, University of Washington, 1996.
84. C. Zhang, *Immersed Interface Method for hyperbolic System of PDEs with Discontinuous Coefficients*, PhD thesis, University of Washington, 1996.

Zhilin Li

Center for Research in Scientific Computation & Department of Mathematics

North Carolina State University, Raleigh, NC 27695, USA

E-mail: zhilin@math.ncsu.edu.